Chapter 9 Fracture behavior of polymers

1. Theoretical Strength

兩個分子之間的引力可以用 Lennard-Jones Potential Energy Function 表示.

$$U = \frac{B}{\gamma^{12}} - \frac{C}{\gamma^{6}} \qquad (1)$$

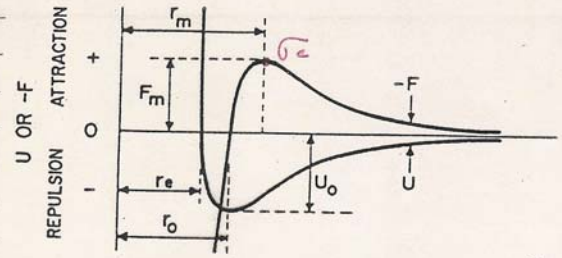

Figure 2.2. Intermolecular energy and force based on the Lennard-Jones 6-12 potential energy function.

利用(1)式可以推導出兩個原子之間的引力和斥力的關係式

$$\sigma = \frac{2\pi\beta_1^2}{\gamma^3}\left(\frac{C}{12} - \frac{B}{9\gamma^6}\right)$$

當 $\sigma = 0$.

$$B = \frac{15}{2} C \gamma_0^6$$

$$\gamma_0 = \left(\frac{2}{15}\frac{B}{C}\right)^{1/6}$$

γ_0 叫做 equilibrium separation

理想 perfect 材料 is Cohesive strength σ_c
(沒有 internal cracks)

$$\sigma_c = \frac{\pi \beta_1^2 C}{9(3)^{1/2} \gamma_0^3}$$

$$E = \left.\frac{\gamma_0 d\sigma}{dr}\right|_{r=r_0} = \frac{1}{2} 9(3)^{1/2} \sigma_c$$

$$\therefore \sigma_c = \frac{E}{7.79}$$

實際上 對 brittle 材料

$$\sigma_c \cong 10^{-3} E$$

最強 is ~~Fiber~~ Carbon Fibers. T-1000

$\sigma_c \cong 10^6$ psi

$E = 40 \times 10^6$ psi

$$\therefore \sigma_c = \frac{E}{40}$$

2. The Elastic Stress Concentration Factor.

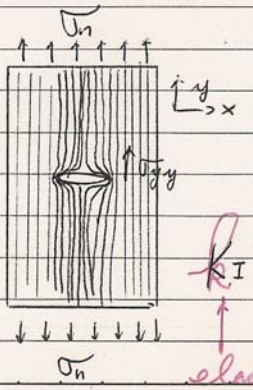

$\sigma_n = 100$ psi

$\sigma_{yy} = 10{,}000$ psi

$$K_I = \frac{\sigma \text{ in the vicinity of defect}}{\sigma_n}$$

K_I ← elastic stress concentration factor

* Crack 附近 Stress 的分佈：

Stress Intensity Factor Solutions

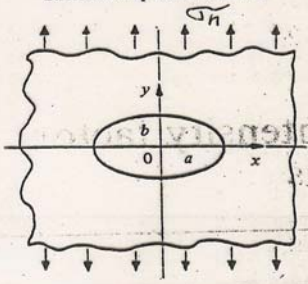

Fig. 4.1 An elliptical hole in a plate

定義 $2B = a+b$

$$m = \frac{a-b}{a+b}$$

$$\alpha = \frac{x}{2B} + \sqrt{\left(\frac{x}{2B}\right)^2 - m}$$

↑ distance parameter

則 由應力分析，可得到在 Crack 附近 Stress 的分佈為

$$\sigma_{yy} = \frac{\tau_2}{2} + \tau_1$$

$$\sigma_{xx} = \frac{\tau_2}{2} - \tau_1$$

where $\tau_1 = \frac{\sigma_n}{2}\left\{1 + \left(\frac{m^2-1}{\alpha^2-m}\right)\left[1 + \left(\frac{m-1}{\alpha^2-m}\right)\left(\frac{3\alpha^2-m}{\alpha^2-m}\right)\right]\right\}$

$$\sigma_2 = \sigma_n \left\{ 1 + \frac{2(1-m)}{\alpha^2 - m} \right\}$$

對於 $x=a$

$$\alpha = \frac{a}{a+b} + \sqrt{\left[\frac{a^2}{(a+b)^2} - \frac{a-b}{(a+b)} \right]} = 1$$

$$\sigma_1 = \frac{\sigma_n}{2} \left\{ 1 + \left(\frac{m^2-1}{1-m} \right) \left[1 + \left(\frac{m-1}{1-m} \right) \left(\frac{3-m}{1-m} \right) \right] \right\}$$

$$\sigma_1 = \frac{\sigma_n}{2} \left(\frac{3+m}{1-m} \right)$$

$$\sigma_2 = \sigma_n \left(\frac{3+m}{1-m} \right)$$

$$\therefore \sigma_{xx} \Big|_{x=a} = 0$$

$$\sigma_{yy} \Big|_{x=a} = \sigma_n \left(1 + \frac{2a}{b} \right)$$

If $a=b$ (~~cuck~~ circle)

$\sigma_{yy} = \sigma(1+2) = 3\sigma_n$

If $\frac{2a}{b} \to \infty$ (for line crack)

$\sigma_{yy} = \infty$ (因此反物取名一對等法)

假設 crack 為橢圓形

The curvature of the ellipse is

$$\rho = \frac{b^2}{a} \qquad \frac{a}{b} = \sqrt{\frac{a}{\rho}}$$

$\sigma_{yy} = \sigma_n \left(1 + 2\sqrt{\frac{a}{\rho}}\right)$

对于 sharp line crack

$b = 0, \quad 2B = a, \quad m = 1$

$\therefore \quad \sigma_1 = \frac{\sigma_n}{2}$

$\sigma_2 = \sigma_n \left(1 + \frac{\alpha}{\alpha^2 - 1}\right)$

$\sigma_{yy} = \frac{\sigma_2}{2} + \sigma_1 = \sigma_n \frac{\alpha^2 + 1}{\alpha^2 - 1}$

where $\alpha = \frac{x}{a} + \sqrt{\left(\frac{x}{a}\right)^2 - 1}$

Let $x = a + r$

$\sigma_{yy} = \sigma_n \left[\left(\frac{a}{2r}\right)^{1/2} + \frac{3}{8}\left(\frac{2r}{a}\right)^{1/2} - \frac{5}{128}\left(\frac{2r}{a}\right)^{\frac{3}{2}} + \cdots \right]$

$r \to 0$

$\sigma_{yy} \simeq \sigma_n \sqrt{\frac{a}{2r}}$

定义 $\sigma_{yy}\sqrt{2\pi r} = K_I$ (Stress intensity factor)

K_I 也就是 the state of stress around the crack.

$K_I = \beta \sigma_n \sqrt{\pi a}$.

对材料特有的 σ_c 当 $\sigma_n = \sigma_c$ 时，则 $K_{Ic} = \sigma_c \sqrt{\pi a}$

stress mx

K_{IC} 叫做 mode I critical stress intensity factor.

上式适用於试件的宽度要够大的情况(没有 edge effect)。在实际应用时，上式必须 modify.

对於 center notch 试件.

σ_n

$$K_{IC} = Y^2 (a/D)\sigma_c{}^2 a$$

$$Y^2 = \pi\left(\frac{2}{\pi}\frac{D}{a}\right)\tan\left(\frac{\pi}{2}\frac{a}{D}\right)$$

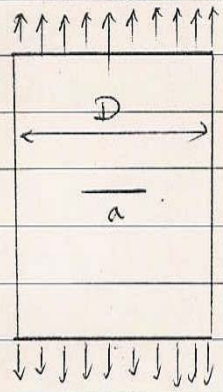

$$Y = 1.77 + 0.22\left(\frac{a}{D}\right) - 0.51\left(\frac{a}{D}\right)^2 + 2.70\left(\frac{a}{D}\right)^3$$

SEN (Single edge notch) 시편

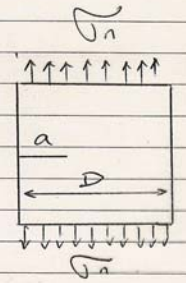

$$K_{Ic}^2 = Y^2 \left(\frac{a}{D}\right) \sigma_n^2 a$$

$$Y^2 \simeq 3.94 \left(\frac{2}{\pi} \frac{D}{a}\right) \tan\left(\frac{\pi}{2} \frac{a}{D}\right)$$

또는 $Y = \sum_0^4 A_n \left(\frac{a}{D}\right)^n$

$$= 1.99 - 0.41 \left(\frac{a}{D}\right) + 18.7 \left(\frac{a}{D}\right)^2 - 38.48 \left(\frac{a}{D}\right)^3 + 53.85 \left(\frac{a}{D}\right)^4$$

3. The Griffith Criterion

The Griffith criterion is defined as that a crack will propagate when decrease in elastic stored energy is at least equal to the energy needed to create new surface.

$$\therefore G_c = \frac{dU}{dA}$$

Energy needed to extend a preexisting crack for an infinitesimal unit area.

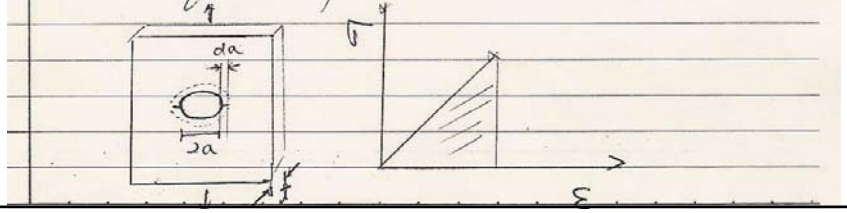

$$dW_E = \frac{1}{2}\sigma \cdot \varepsilon \cdot dV$$

$$= \frac{1}{2}\sigma \cdot \frac{\sigma}{E} \cdot 2\pi a\, da \cdot t$$

$$dW_S = \gamma^e \times da \times t \times 4$$

$$\frac{dW_E}{da} = \frac{\pi a t \sigma^2}{E}$$

$$\frac{dW_S}{da} = 4t\gamma^e$$

$$\frac{dW_E}{da} \geq \frac{dW_S}{da}$$

$$4t\gamma^e \doteq \frac{\pi a t \sigma_c^2}{E} \qquad \text{at critical point}$$

$$\therefore \sigma_c = \geq \sqrt{\frac{\gamma^e E}{\pi a}}$$

$$\therefore G_c = \frac{dU}{dA} = \frac{dU}{t\,da} = \frac{\gamma^e 4 * da}{t\,da}$$

$$= 4\gamma^e.$$

$$\therefore \sigma_c \sqrt{\pi a} = \sqrt{G_c E} = K_c.$$

$$G_c = \frac{K_c^2}{E}$$

For thick sheet

$$\sigma_c = 2\sqrt{\frac{\gamma E}{\pi a(1-\nu^2)}}$$

where ν is the poisson ratio.

$$\therefore G_c = \frac{K_c^2(1-\nu)^2}{E}$$

- Compact tension specimen (CTS)

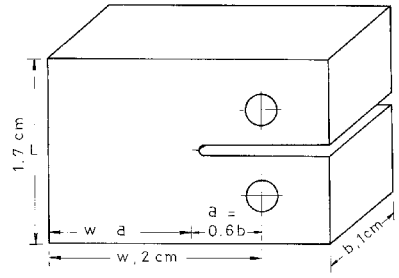

Figure 1 Rectangular compact tension specimen used for fracture test

$$G_{IC} = Y^2 P_c^2 a / b^2 w^2 E \qquad (1)$$

where P_c is the load at crack initiation, a is the crack length, E is Young's modulus, w is the width of specimen, b is the thickness of specimen, and Y is the geometry factor given by

$$Y = 29.6 - 186\,(a/w) + 656(a/w)^2 - 1017\,(a/w)^3 + 639\,(a/w)^4$$

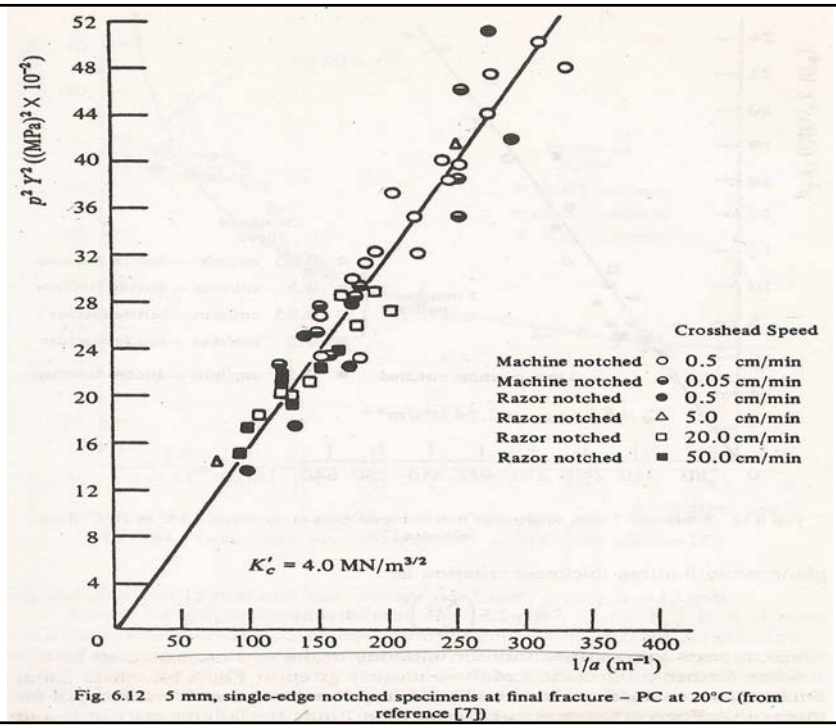

Fig. 6.12 5 mm, single-edge notched specimens at final fracture – PC at 20°C (from reference [7])

K_{c1} Values at 20°C

Material	K_{c1} (MPa$\sqrt{\text{m}}$)
PMMA	0.7–1.6
PS	0.7–1.1
PC	2.2
PES (Polyethersulphone)	1.2
HIPS	1.0–2.0
ABS	2.0
PVC	2.0–4.0
PP	3.0–4.5
PE	1.0–6.0
POM (Acetal)	≃4
PA (Nylon)	2.5–3.0
Epoxies	0.6
Polyesters	0.6
PET (Polyethylene terephthalate)	≃5

- **Fracture surface of CTS speciemen of $Cr(acac)_3$-toughening epoxy resins**

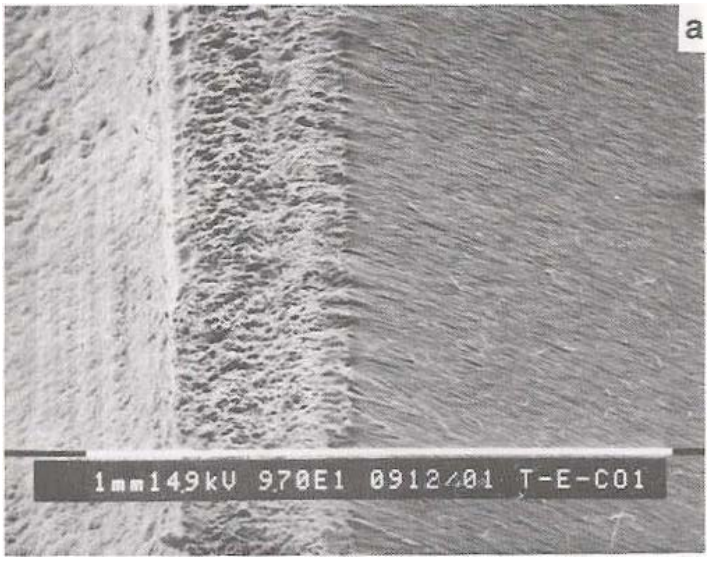

TGDDM/DDS epoxy resin

TGDDM/DDS/1%$Co(acac)_3$

TGDDM/DDS/1%$Cr(acac)_3$

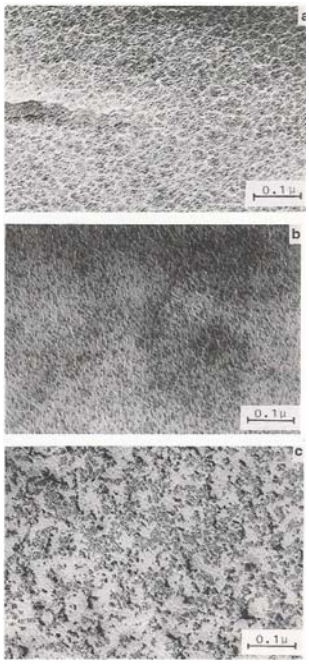

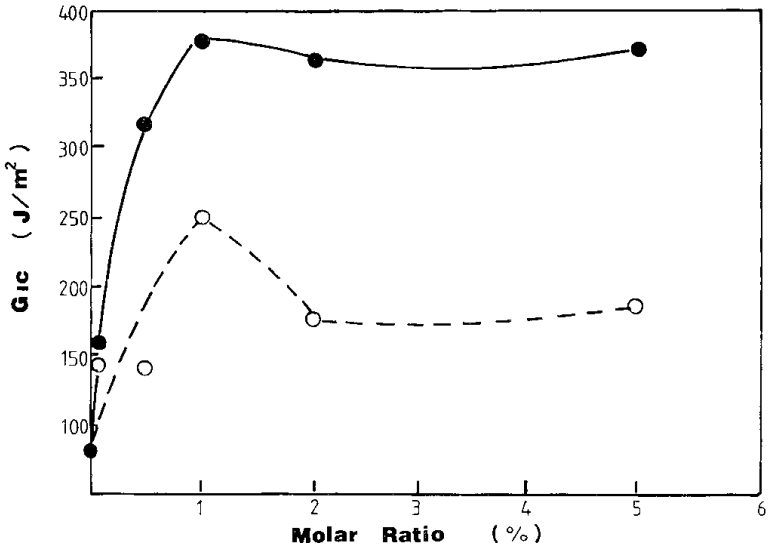

Figure 16 G_{Ic} value of modified TGDDM/DDS epoxy resins as a function of molar ratio of incorporated (●) $Cr(acac)_3$ and (○) $Co(acac)_3$

- Proposed interaction mechanism between $Cr(acac)_3$ and cured TGDDM/DDS network

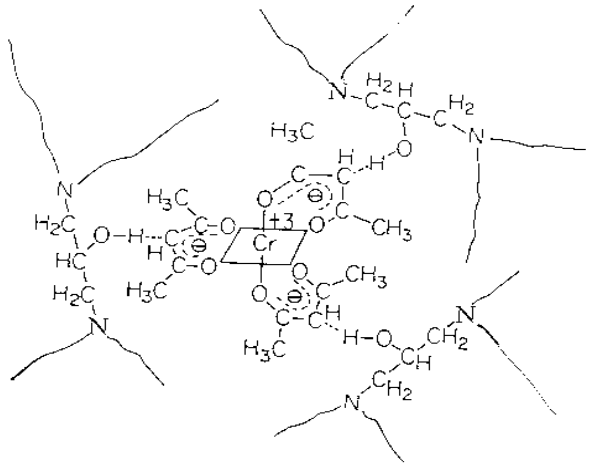

$Cr(acac)_3$ has been shown to be easily prepared by pH control with basic media in a solution of chromium(III) chloride and acetylacetone[15]. The reaction is:

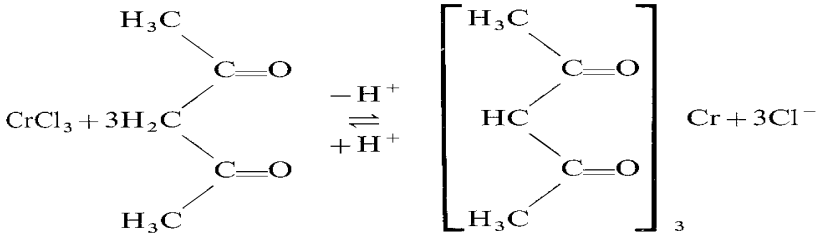

The $(acac)^-$ ligand exists in resonance forms which are best represented as:

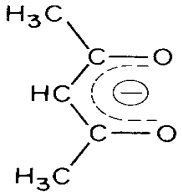

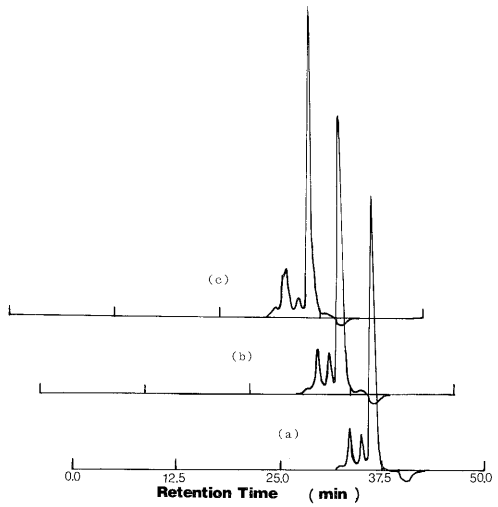

Figure 22 G.p.c. chromatograms of (a) DGEBA monomers (EEW = 187 g mol^{-1}) and their mixtures with (b) 1% $Co(acac)_3$ and (c) 1% $Cr(acac)_3$

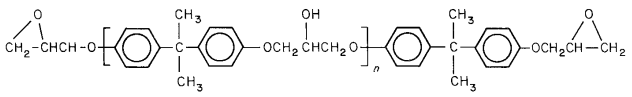

Figure 23 Typical chemical structure of DGEBA epoxy resin

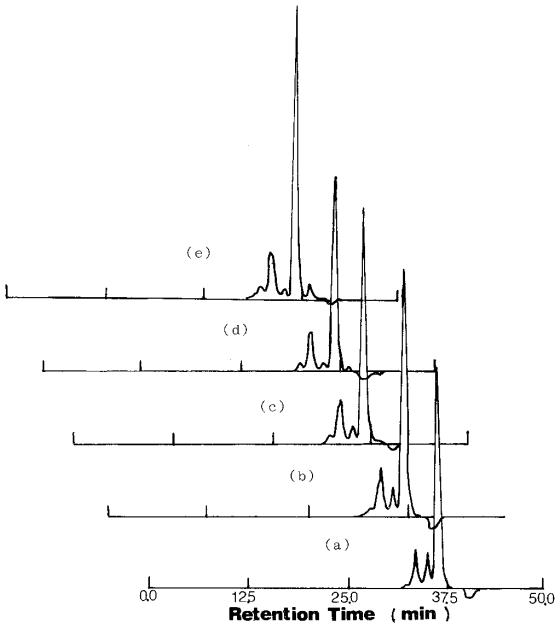

Figure 24 G.p.c. chromatograms of DGEBA monomers (*EEW* = 187 g mol^{-1}) mixed with various molar ratios of $Cr(acac)_3$: (a) 0.5%, (b) 1%, (c) 2% and (d) 5%

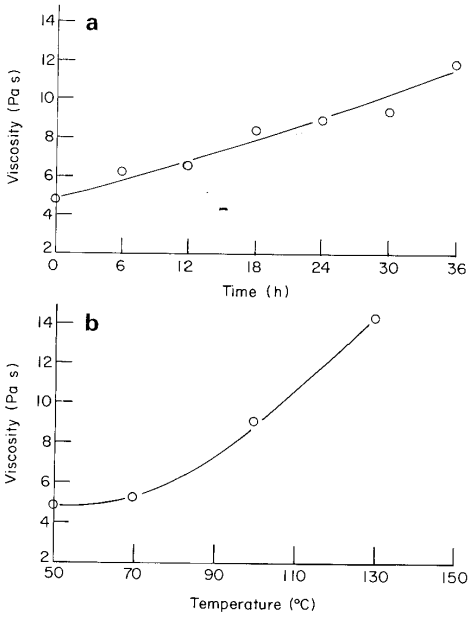

Figure 1 Viscosity of DGEBA resins incorporating 1 mol% $Cr(acac)_3$ measured at 30°C as functions of (a) mixing time at 100°C and (b) temperature at which it was mixed for 24 h

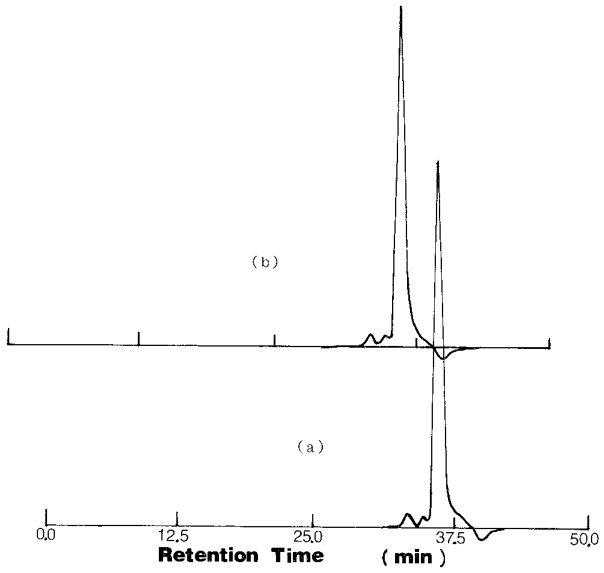

Figure 25 G.p.c. chromatograms of (a) DGEBA monomers (EEW = 174 g mol^{-1}) and (b) their mixture with 1% $Cr(acac)_3$

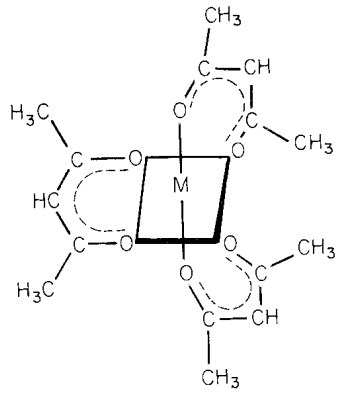

where M = Cr or Co. The i.r. spectra of pure $Cr(acac)_3$ and $Co(acac)_3$ are shown in *Figure 5*. The notable difference between the two spectra is that the C–O bending peak[12] is at 600 cm^{-1} for $Cr(acac)_3$ but at 640 cm^{-1} for $Co(acac)_3$. Both Cr and Co are in the first transition metal series. However, the radius of Co^{3+} is 0.53 Å whereas that of Cr^{3+} is 0.57 Å, as derived from the observed interatomic distances in the fluorides[13].

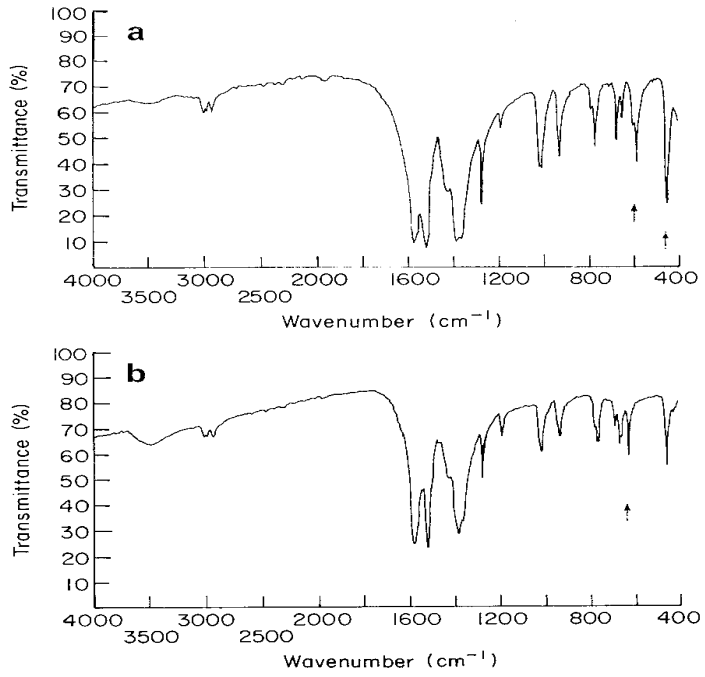

Figure 5 I.r. spectra of (a) $Cr(acac)_3$ and (b) $Co(acac)_3$

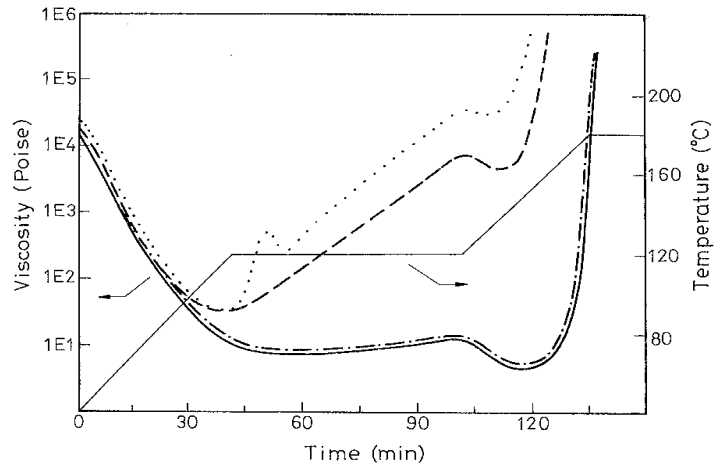

Fig. 6. The viscosity of Gr/Ep prepregs prepared by various epoxy formulations as functions of curing time and indicated temperature schedule; (—) TGDDM/DDS, (—·—) TGDDM/DDS/1%$Cr(acac)_3$, (- - -) TGDDM/DDS/BF_3MEA, and (· · ·) TGDDM/DDS/BF_3MEA/1%$Cr(acac)_3$.

The cross section of unidirectional Gr/Ep laminates parepared by (a) TGDDM/DDS, and (b) TGDDM/DDS/$Cr(acac)_3$

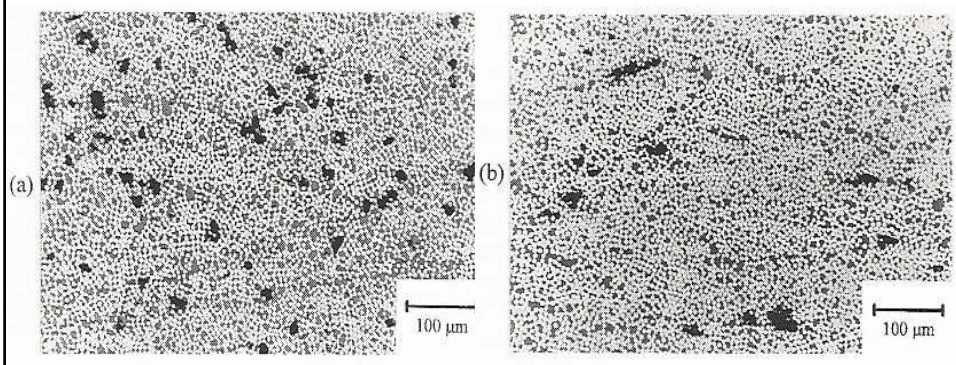

The typical cross section of unidirectional Gr/Ep laminates

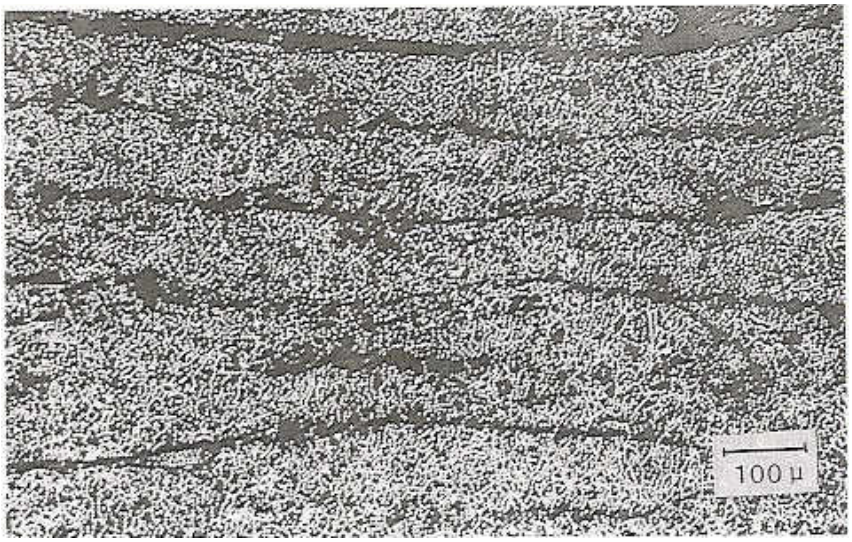

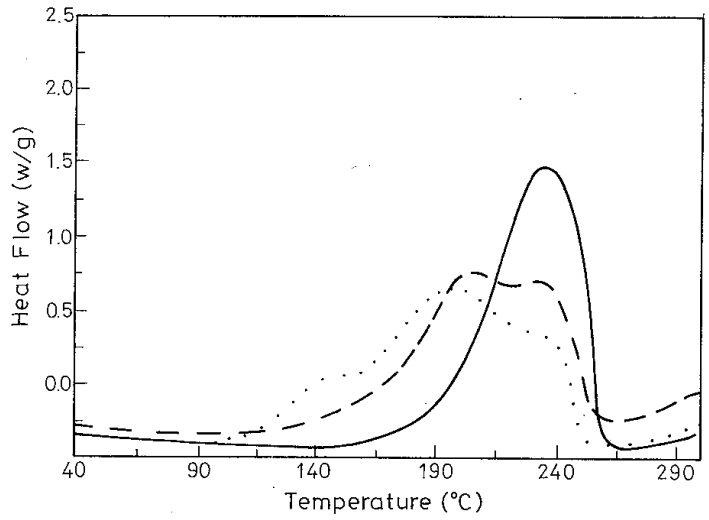

Fig. 1. DSC spectra of (—) TGDDM/DDS, (- - -) TGDDM/DDS/BF_3MEA, and (· · ·) TGDDM/DDS/BF_3MEA/1% $Cr(acac)_3$ epoxy formulations.

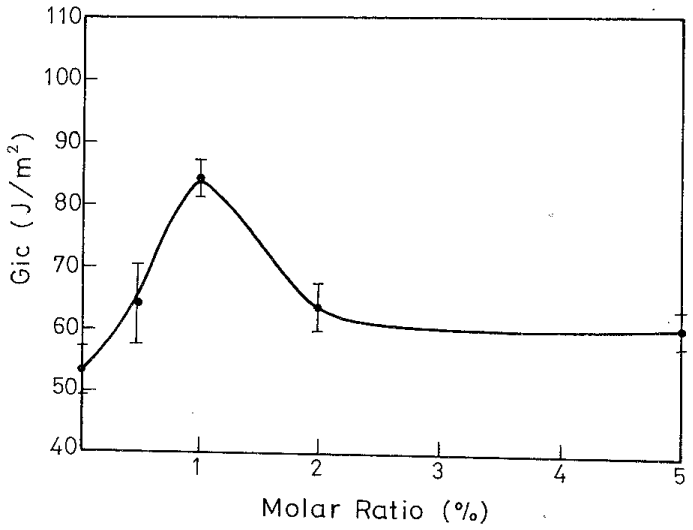

Fig. 7. G_{IC} of TGDDM/DDS/BF_3MEA epoxy resins as function of molar ratio of incorporated $Cr(acac)_3$.

4. Double Cantilever Beam (DCB) Specimen:

在 fracture tests 中，依施力的方向可分为3种破坏模式

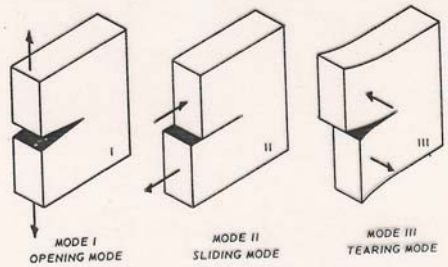

以 Mode I 的试片做实验，我们可得到

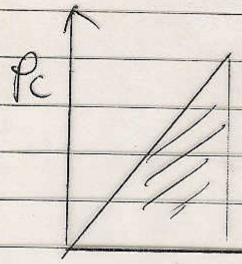

$$U = \frac{P_c \delta}{2}$$

根据 $C = \frac{\delta}{P}$ (compliance)

$$U = P_c^2 C / 2$$

$$G_{Ic} = \frac{dU}{dA} = \frac{d\left(\frac{P_c^2 C}{2}\right)}{dA}$$

$$= \frac{P_c^2}{2B}\left(\frac{dC}{da}\right)_P$$

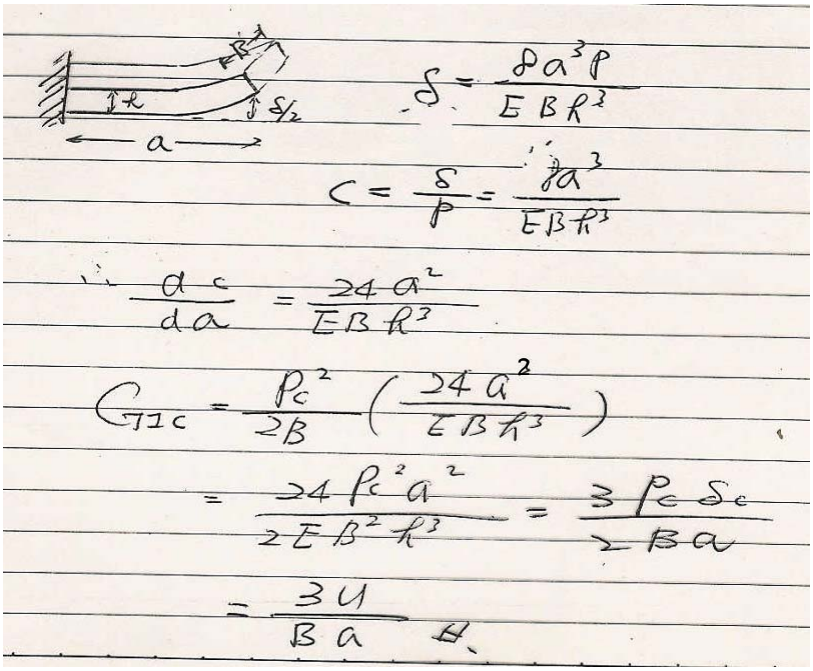

$$\delta = \frac{8a^3P}{EBR^3}$$

$$C = \frac{\delta}{P} = \frac{8a^3}{EBR^3}$$

$$\frac{dC}{da} = \frac{24a^2}{EBR^3}$$

$$G_{IC} = \frac{P_c^2}{2B}\left(\frac{24a^2}{EBR^3}\right)$$

$$= \frac{24P_c^2a^2}{2EB^2R^3} = \frac{3P_c\delta_c}{2Ba}$$

$$= \frac{3U}{Ba}$$ #

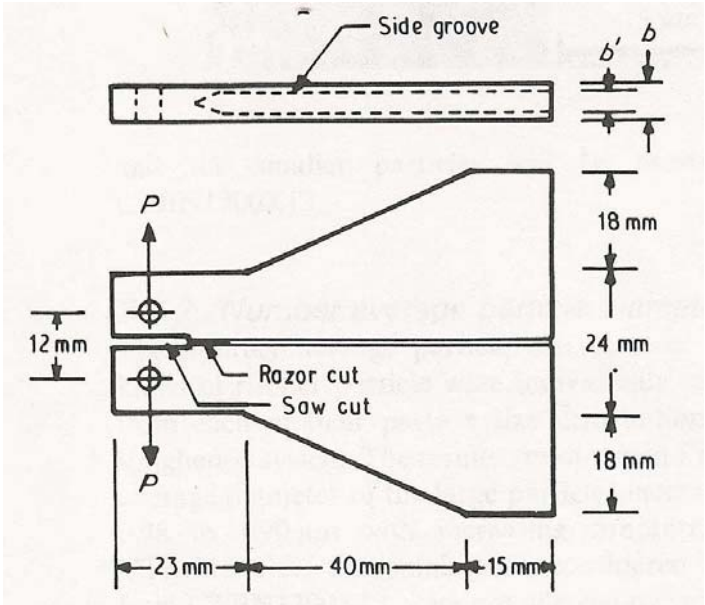

Figure 1 Tapered-double cantilever beam specimen used for fracture energy measurement.

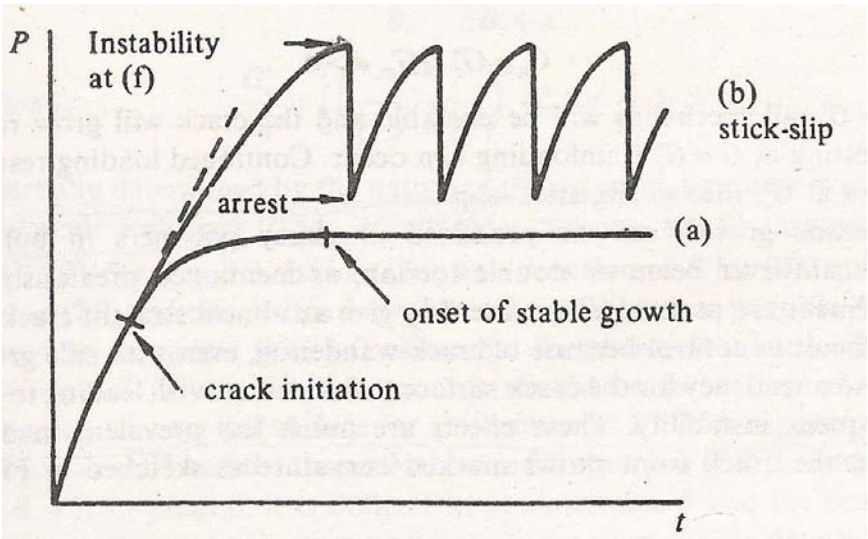

Fig. 7.5 Stable crack growth and stick–slip at u constant

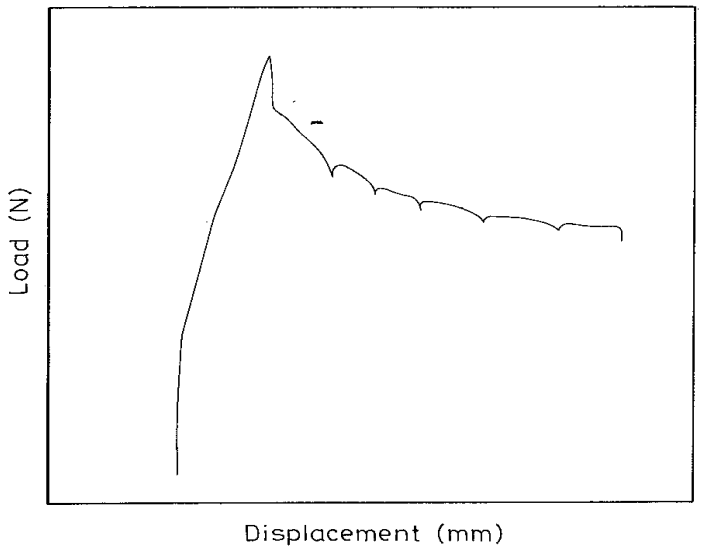

Fig. 8. A typical figure of load versus crack open displacement during interlaminar fracture test of Gr/Ep laminates.

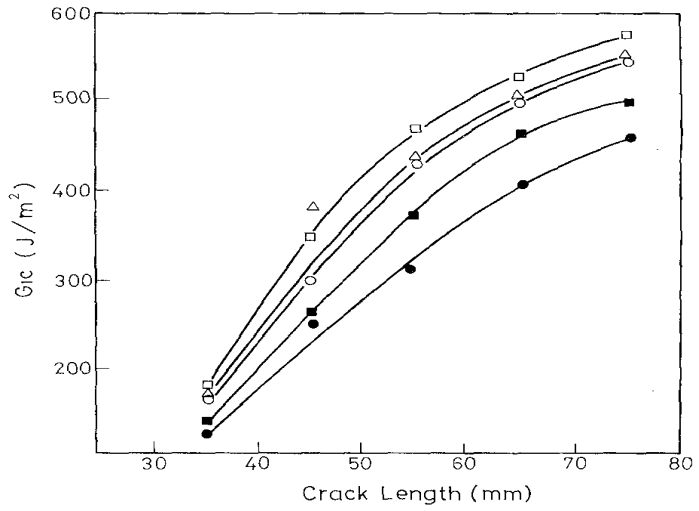

Fig. 9. G_{IC} of the Gr/Ep $[0]_{24}$ laminates prepared by TGDDM/DDS/BF_3MEA epoxy formulations incorporating various amount of $Cr(acac)_3$; (•) 0, (■) 0.5 mol%, (□) 1 mol%, (Δ) 2 mol%, and (○) 5 mol%.

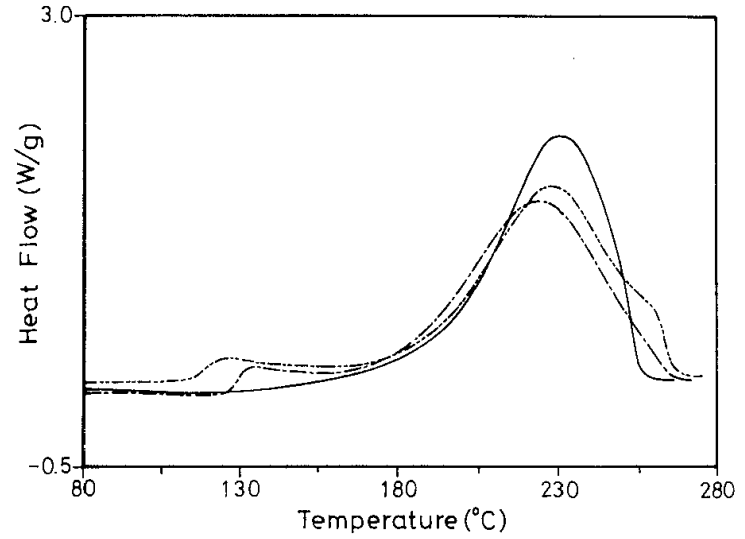

Fig. 1. DSC spectra of (——) TGDDM/DDS, (-·-·-) TGDDM/DDS/$C_{11}Z$, and (- - -) TGDDM/DDS/$C_{11}Z$/$Cr(acac)_3$.

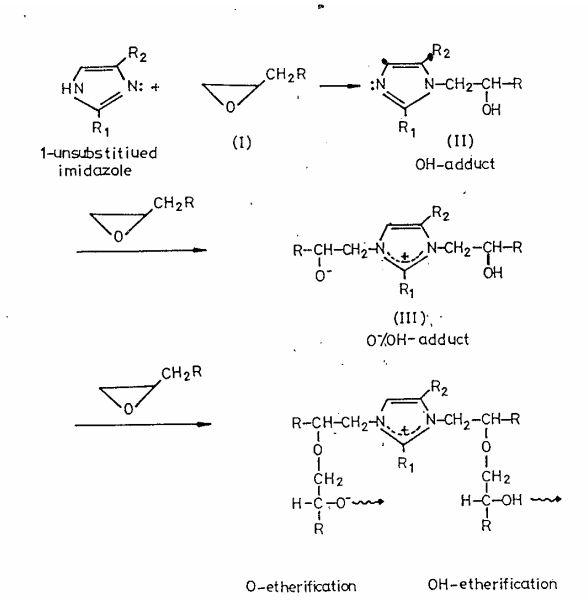

Figure 2. Reaction mechanism of TGDDM with $C_{11}Z$ (8).

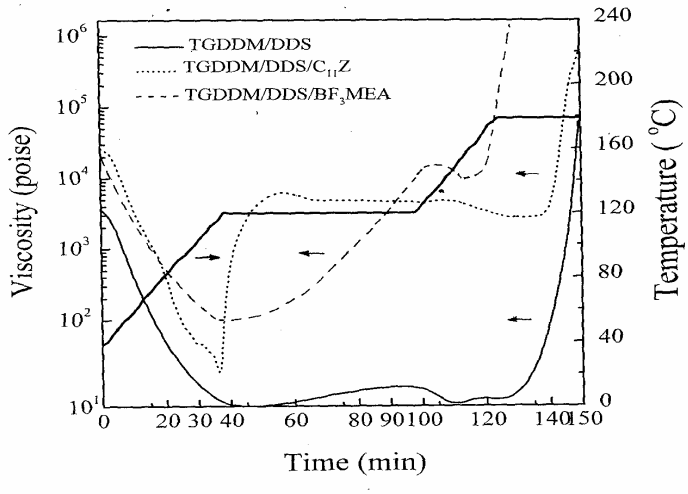

Figure 4. The viscosity of various epoxy matrices as functions of curing time and the indicated temperature schedule used to prepare the Gr/Ep laminates.

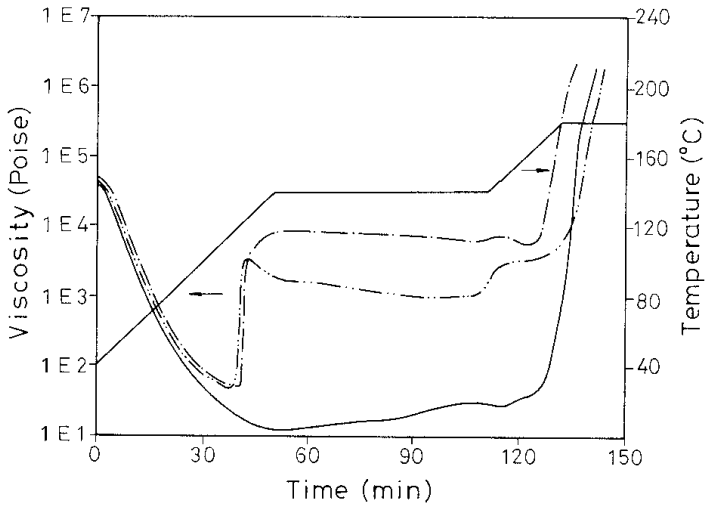

Fig. 5. The viscosity of Gr/Ep prepregs prepared by various epoxy formulations as functions of curing time and indicated temperature schedule: (——) TGDDM/DDS, (—··—) TGDDM/DDS/$C_{11}Z$, and (-·-) TGDDM/DDS/$C_{11}Z$/$Cr(acac)_3$.

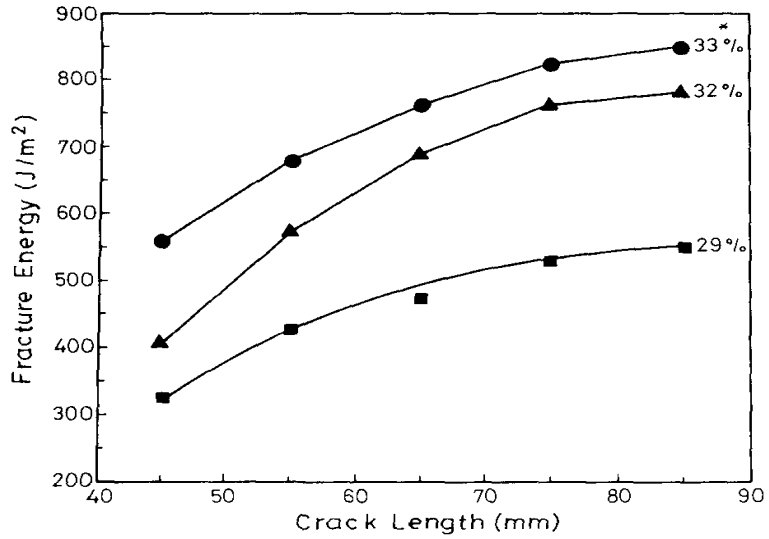

Fig. 8. G_{IC} of the Gr/Ep [O] 24 laminates prepared by various epoxy formulations: (■) TGDDM/DDS/BF_3MEA, (▲) TGDDM/DDS/$C_{11}Z$, and (●) TGDDM/DDS/$C_{11}Z$/$Cr(acac)_3$.
** Resin content.*

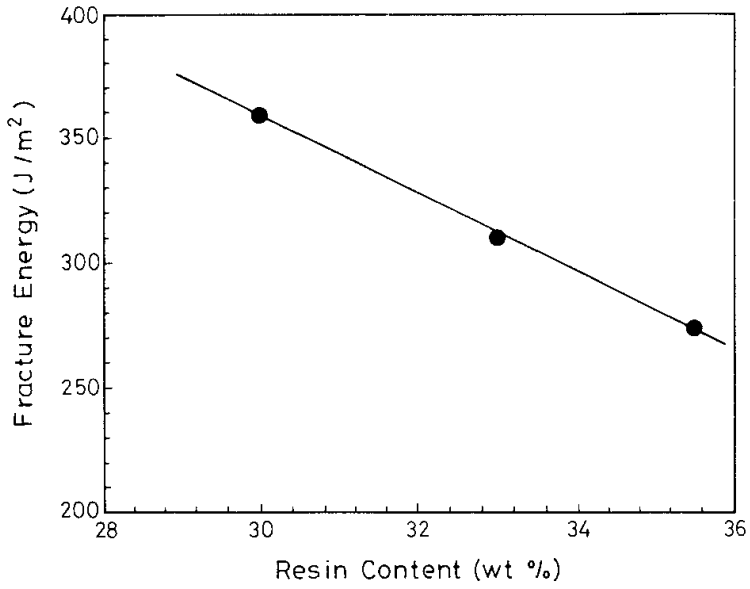

Fig. 9. G_{IC} at 45 mm crack length vs. the resin content of the Gr/Ep [O] 24 laminates prepared by TGDDM/DDS incorporating various amounts of fumed silica (12).

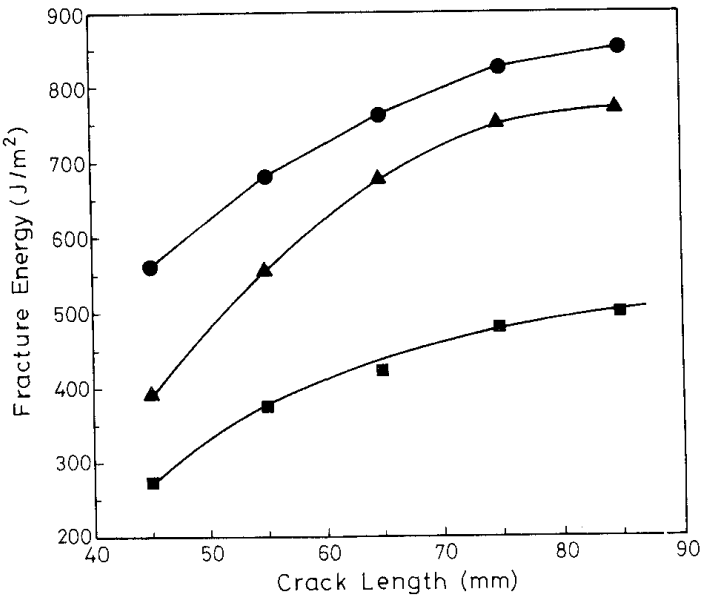

Fig. 10. G_{IC} of the same laminates as those in Fig. 8 but with the resin content adjusted to 33 wt%.

Table 2. Fracture Data of Various Epoxy Formulations and Their Gr/Ep Laminates.

Formulation	(1) G_{IC} of Neat Resin (J/m^2)	(2) G_{IC} of Laminates (J/m^2)	(1)−(2) (J/m^2)	Plastic Zone Diameter (μm)
TGDDM/DDS/BF_3MEA	55 ± 5	270 ± 7	215 ± 12	6.3
TGDDM/DDS/$C_{11}Z$	128 ± 14	392 ± 22	264 ± 36	9.6
TGDDM/DDS/$C_{11}Z$/$Cr(acac)_3$	369 ± 17	560 ± 22	191 ± 39	16.3
		Average 223		

Fiber bridging contribution

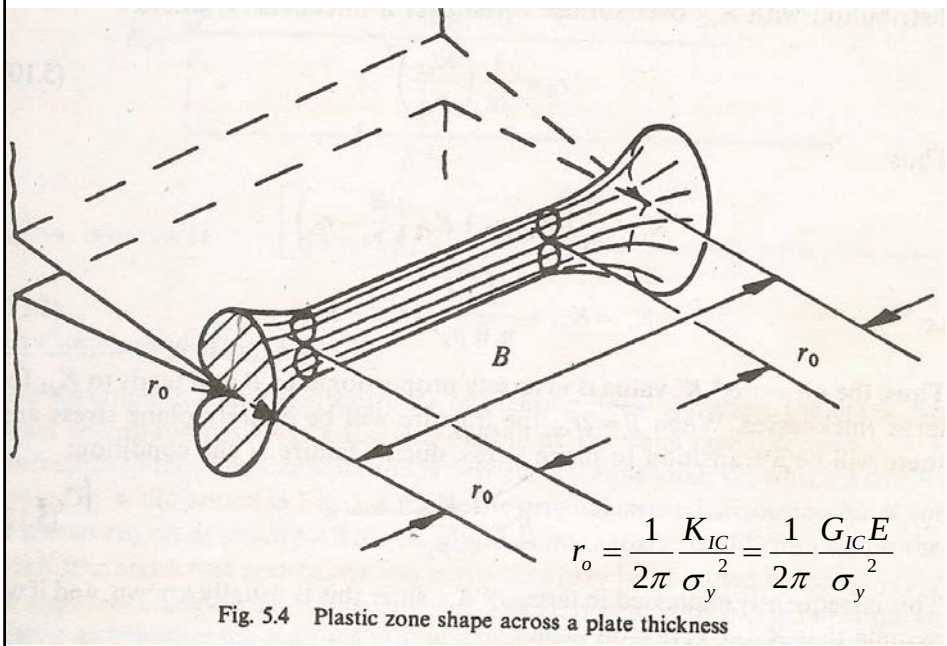

Fig. 5.4 Plastic zone shape across a plate thickness

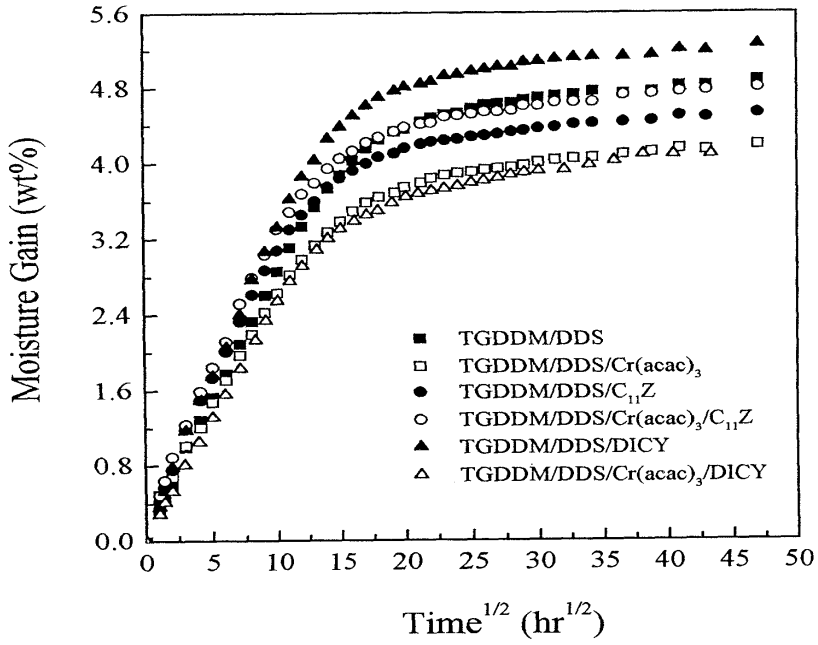

Fig. 3. Moisture gain of various epoxy resins at 60°C/100%RH as a function of square root of time.

Table 3. Moisture Absorption Data of Various Epoxy Resins at 60°C/100%RH.

Resin Formulations	M_m (wt%)	D_n (× 10^3mm/h)	[OH]^a ($I_{3500cm}^{-1}/I_{850cm}^{-1}$)
TGDDM/DDS	4.82	3.42	1.74
TGDDM/DDS/Cr(acac)$_3$	4.15	4.39	1.22
TGDDM/DDS/C$_{11}$Z	4.50	4.03	1.21
TGDDM/DDS/C$_{11}$Z/Cr(acac)$_3$	4.76	3.76	0.89
TGDDM/DDS/DICY	5.20	3.62	1.25
TGDDM/DDS/DICY/Cr(acac)$_3$	4.09	3.18	0.78

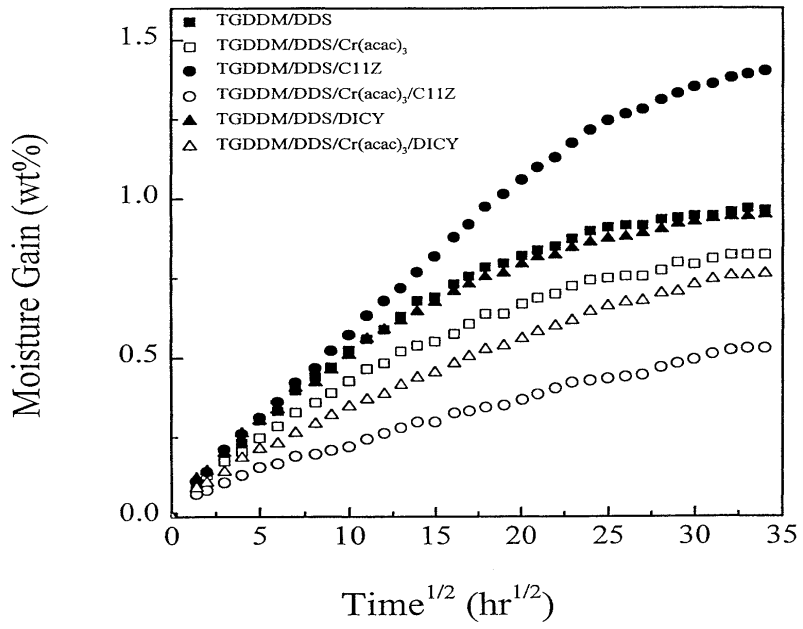

Fig. 1. Moisture gain of various unidirectional Gr/Ep laminates at 60°C/100%RH as a function of square root of time.

Table 2. Moisture Absorption Data of Various Gr/Ep Laminates at 60°C/100%RH.

Epoxy Formulations	M_m[a] (wt%)	Resin Content (wt%)	M_m[b] (wt%)	D	D_r (× 10^3mm²/h)	D_{11}
TGDDM/DDS	0.969	21	4.61	2.65	43.2	11.3
TGDDM/DDS/ $Cr(acac)_3$	0.823	22	3.74	2.75	38.4	10.6
TGDDM/DDS/$C_{11}Z$	1.402	33	4.25	3.01	12.3	5.08
TGDDM/DDS/ $C_{11}Z/Cr(acac)_3$	0.530	27	1.96	1.99	14.7	5.48
TGDDM/DDS/DICY	0.948	24	3.95	3.13	30.5	9.16
TGDDM/DDS/ $DICY/Cr(acac)_3$	0.762	25	3.05	2.61	23.1	7.21

[a]The moisture gain by laminates after 1200 h.

[b]The moisture gain by resin matrix after 1200 h, assuming only resin matrix absorbed moisture.

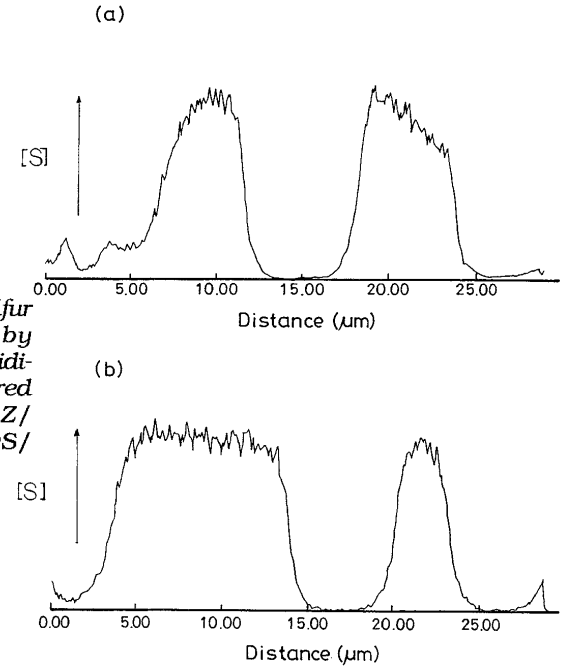

Fig. 5. Typical line-scanning sulfur concentration distributions by EPMA on the cross-section of unidirectional Gr/Ep laminates prepared from (a) TGDDM/DDS/$C_{11}Z$/$Cr(acac)_3$ and (b) TGDDM/DDS/$Cr(acac)_3$.

CONCLUSIONS

The addition of both 1 mol% $Cr(acac)_3$ and 1 phr $C_{11}Z$ to the TGDDM/DDS epoxy formulation was found to have a synergistic effect on reducing the moisture absorption of the prepared laminate, but not of the neat resin. The synergistic effect was attributed to the separation of the low moisture absorptive TGDDM/$C_{11}Z$-richer network and TGDDM/DDS/$Cr(acac)_3$-richer network to some extent in the epoxy matrix during the lamination process. When the preheating temperature was decreased during lamination to increase the resin viscosity, the synergistic effect of additives to reduce the moisture absorption of prepared laminates became more pronounced. In addi-

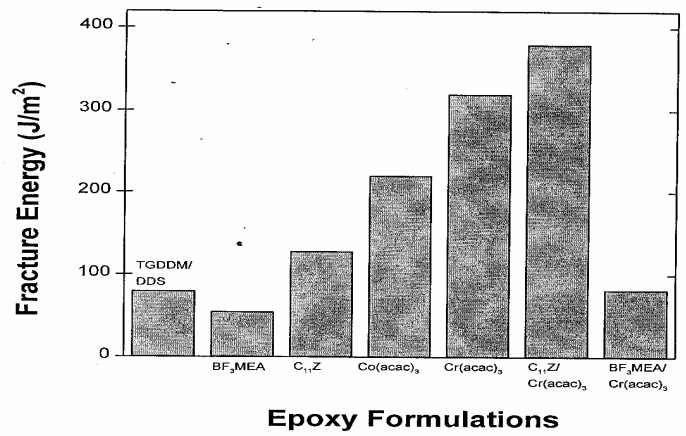

Figure 3. Fracture energy of cured epoxy resins prepared by various epoxy formulations; listing from left to right: 1.TGDDM/DDS, 2.TGDDM/DDS/BF_3MEA, 3.TGDDM/DDS/$C_{11}Z$, 4.TGDDM/DDS/Co(acac)$_3$, 5.TGDDM/DDS/Cr(acac)$_3$, 6.TGDDM/DDS/$C_{11}Z$/Cr(acac)$_3$, and 7.TGDDM/DDS/BF_3MEA/Cr(acac)$_3$.

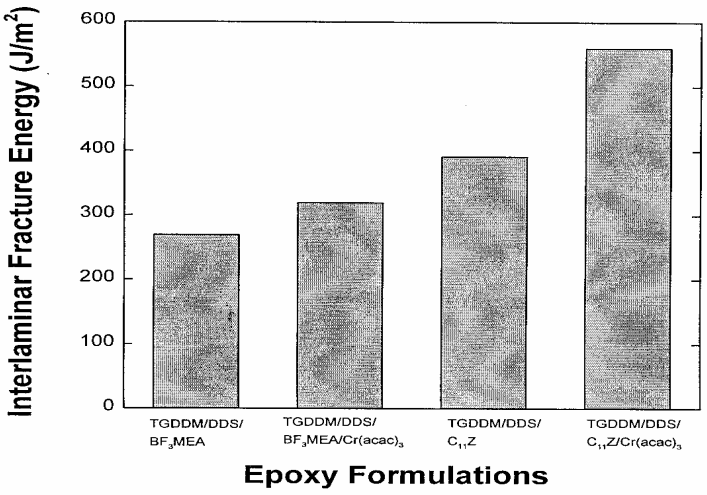

Figure 5. Interlaminar fracture energy at 45 mm crack length of Gr/Ep $[0]_{24}$ laminates prepared by various epoxy formulations. All the data have been adjusted to the same resin content at 30 wt%.

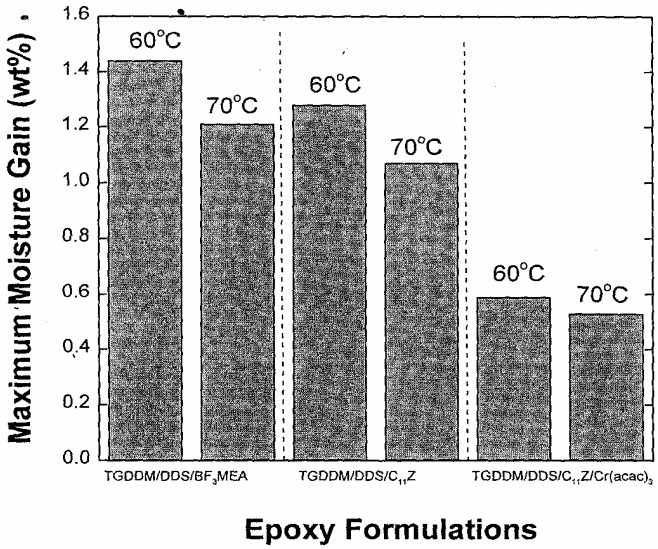

Figure 6. Maximum moisture gains of Gr/Ep $[0]_{16}$ laminates prepared by various epoxy formulations under moisture absorption experiments at 60℃/100%RH and 70℃/100%RH. All the data have been adjusted to the same resin content at 30 wt%.

- The effect of crack speed on the measurement of fracture toughness for polymers

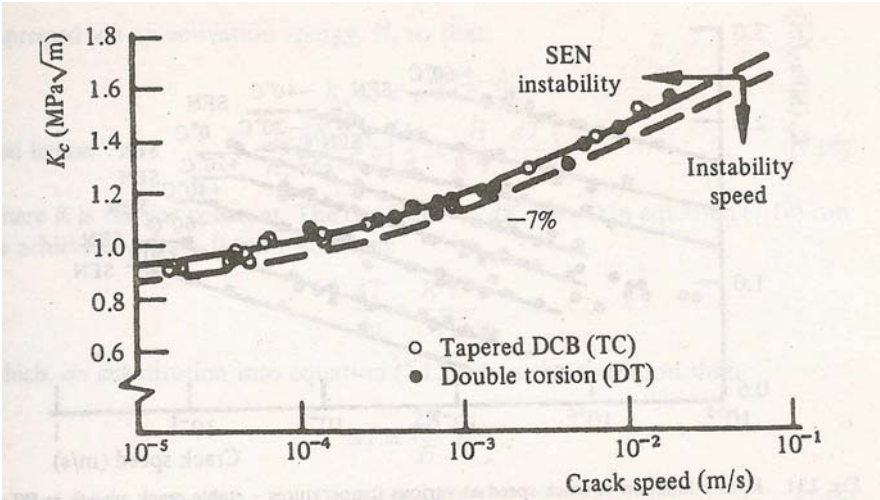

Fig. 7.10 A comparison of tapered DCB and double torsion data for PMMA at 20°C (from reference [6])

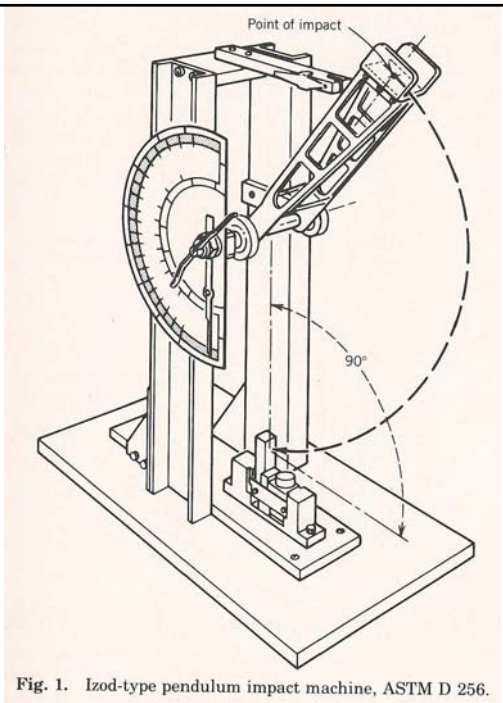

Fig. 1. Izod-type pendulum impact machine, ASTM D 256.

- High speed fracture test (~3.4 m/s)

1. Izod impact test of polymers

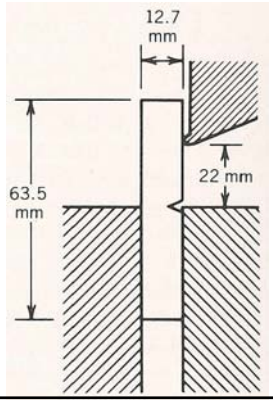

The energy absorbed by the specimen E_S is found by

$$E_S = E_I - E_R - E_F - E_W$$

where E_I is the initial energy available, E_R the energy at the maximum angular travel, E_F the energy dissipated by friction, and E_W the energy to remove the broken section. The last is usually small; E_F can be found by performing the test without a specimen in place. Machines of this type are usually equipped with a dial with calibration marks mounted in the plane of rotation in such a way that E_I and E_R can be read directly. An "instrumented" pendulum machine is equipped with a load cell, usually a piezoelectric device for high frequency response, mounted on the striker or on the mounting block to which the specimen vise is attached. The electric signal from the load cell is amplified, digitized, and recorded by electronic memory. The energy is calculated from the load–time relationship by a computer connected to the instrument. The total energy can be displayed by a digital readout, or the entire load–time trace can be displayed on a cathode-ray tube screen. In the latter instance, a microcomputer is attached and the information can be processed as desired.

Table 11.2 Izod impact strengths of several plastics[a, b](3)

Polymer	Impact Strength
Polystyrene	0.25–0.4
High-impact polystyrene (Hips)	0.5–4
ABS plastics	1–8
Epoxy resin (no filler)	0.2–1.0
Epoxy resin (glass-fiber-filled)	10–30
Cellulose acetate	0.4–5.2
Poly(methyl methacrylate)	0.3–0.5
Phenol–formaldehyde plastics	0.20–0.36
Poly(vinyl chloride)	0.4–1
High-impact poly(vinyl chloride)	10–30

[a] *Modern Plastics Encyclopedia* (1973); Lannon (1967).
[b] ASTM test D256 was followed, and the values reported have the units ft · lb/in. of notch.

2. Charpy impact test of polymers

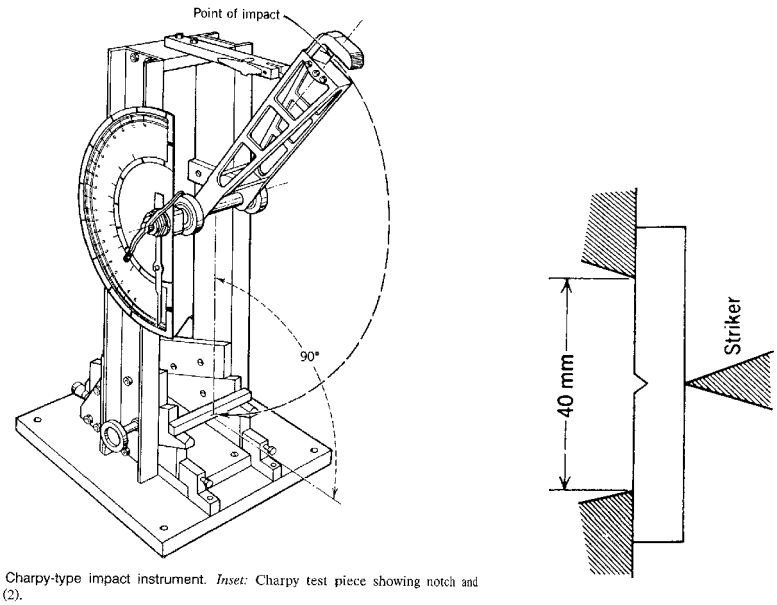

Figure 11.11 Charpy-type impact instrument. *Inset:* Charpy test piece showing notch and point of striker (2).

Table 11.3 Impact resistance of ABS polymers at 30°C (16)

Sample Number	Composition of Rubber Component		T_g of Rubber Component, °C	Charpy Impact Strength, kg · cm/cm^2
	BD[a]	ST[b]		
1	35	65	40	0.75
2	55	45	−20	18
3	65	35	−35	30
4	100	0	−85	40

[a] Polybutadiene.
[b] Poly(styrene–*stat*–acrylonitrile).

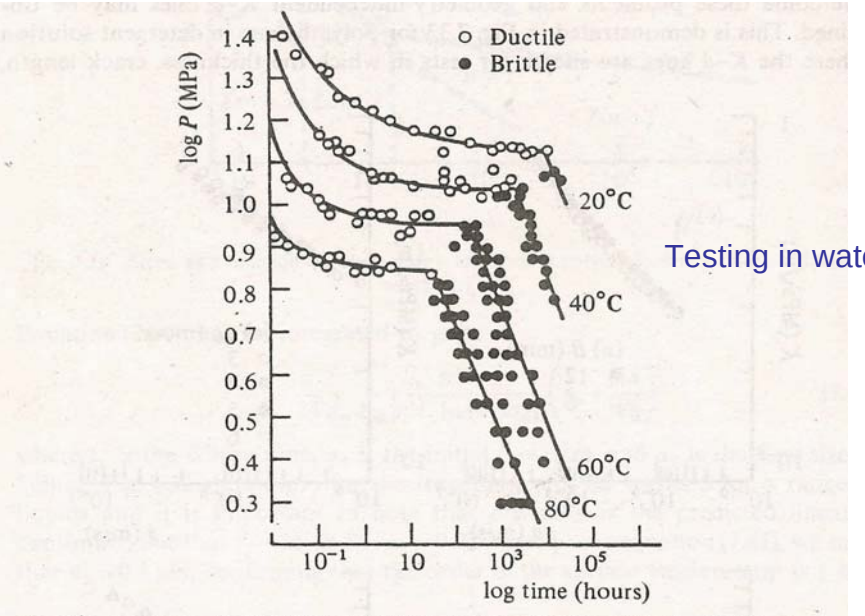

Testing in water

Fig. 7.34 Ductile and brittle failure in HDPE pipe (data kindly supplied by BP Chemicals Limited)

CTBN liqud rubber-toughening epoxy resins

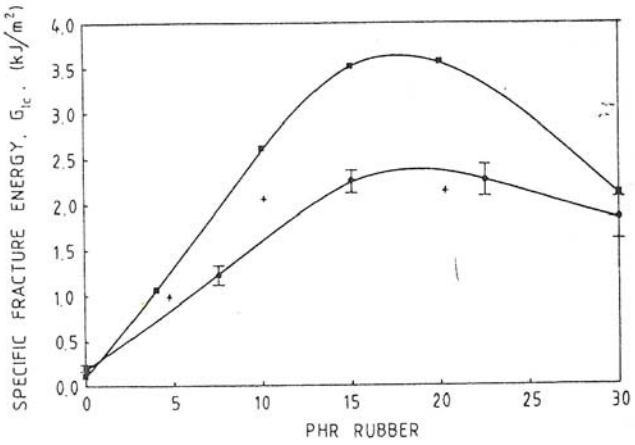

Fig. 1. Variation of specific fracture energy, G_{Ic}, with rubber content. (+) Yee and Pearson;[88] (■) Bascom *et al.*;[16] (●) present work.

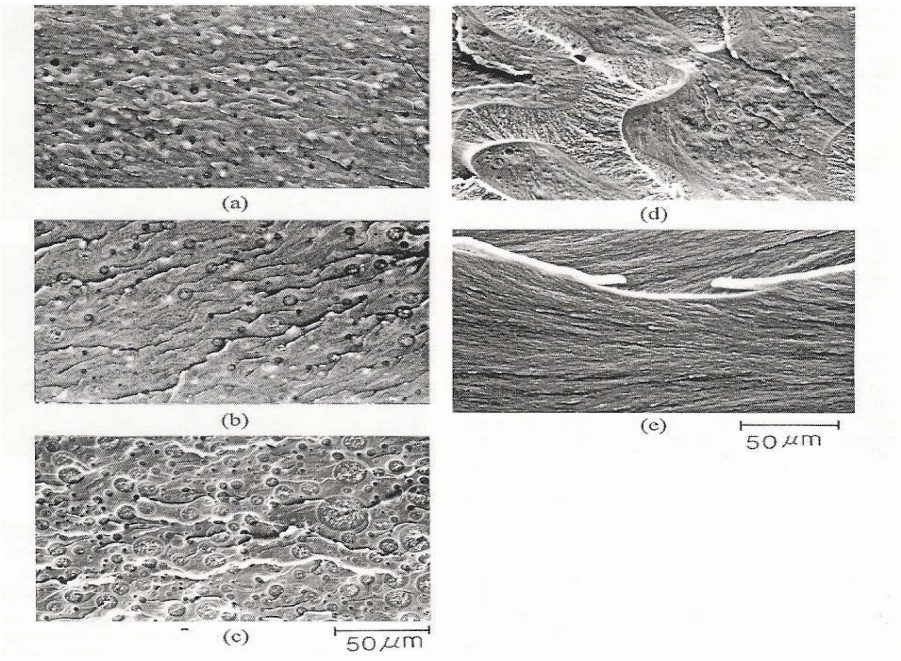

Figure 1 SEM micrographs of the fracture surfaces of DGEBA/EDA epoxy resins incorporating the following amounts of CTBN rubber: (a) 5, (b) 10, (c) 20, (d) 30, and (e) 50 phr.

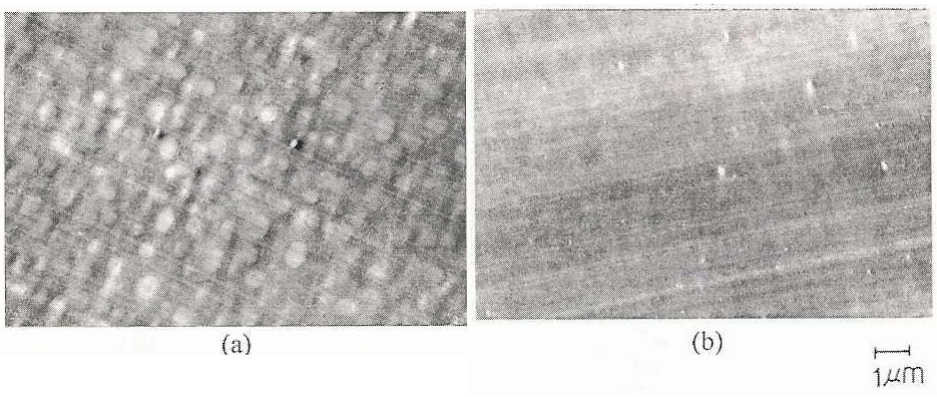

Figure 2 TEM micrographs of OsO_4-stained DGEBA/EDA epoxy resins incorporating the following amounts of CTBN rubber: (a) 50 and (b) 70 phr.

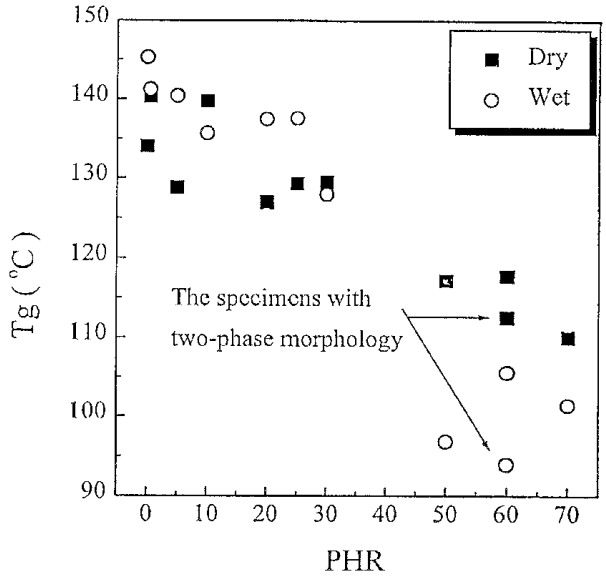

Figure 9 T_g of rubber-modified DGEBA/EDA epoxy resins as a function of the CTBN content: (■) without moisture absorption and (○) after moisture saturation at 60°C and 100% RH.

Core–Shell Particles Designed for Toughening Epoxy Resins. I. Preparation and Characterization of Core–Shell Particles

KING-FU LIN, YEOW-DER SHIEH

Institute of Materials Science and Engineering, National Taiwan University, Taipei, Taiwan 10617, Republic of China

Table I Recipes of First-Stage Soapless Emulsion Polymerization for Preparation of BA Core with and without EGDMA Crosslinking Agent

Component	L-BA	C-BA
BA (g)	30	30
Water (g)	820	820
KPS (g)	0.87	0.87
EGDMA (g)	0	0.6

Table II Recipes of Second-Stage Seeded Emulsion Polymerization for Preparation of Variety of BA/MMA CSPs with Either Crosslinked Core or Crosslinked Shell

	C Series							L Series				
Component	C0	C1	C2	C3	C4	C5	C6	L0	L1	L2	L3	L4
L-BA (g)	780	780	780	780	780	780	780	—	—	—	—	—
C-BA (g)	—	—	—	—	—	—	—	780	780	780	780	780
MMA (g)	27.5	25.5	23.5	21.5	19.5	15.5	0	27.5	25.5	23.5	21.5	15.5
GMA (g)	0	2	4	6	8	12	27.5	0	2	4	6	12
(mol %)[a]	(0)	(5)	(10)	(16)	(22)	(29)	(100)	(0)	(5)	(10)	(16)	(29)
EGDMA (g)	0.6	0.6	0.6	0.6	0.6	0.6	0.6	—	—	—	—	—
KPS (g)	0.2	0.2	0.2	0.2	0.2	0.2	0.2	0.2	0.2	0.2	0.2	0.2

[a] Molar percentage of GMA.

TEM micrographs of vacuum dried CSP's

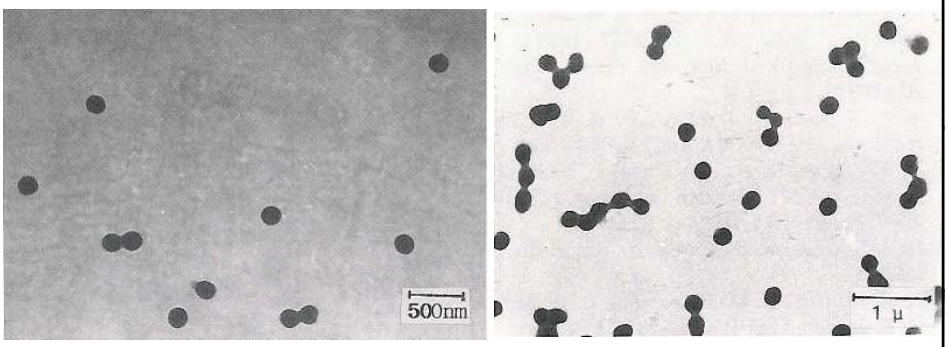

C0 CSP

C3 CSP

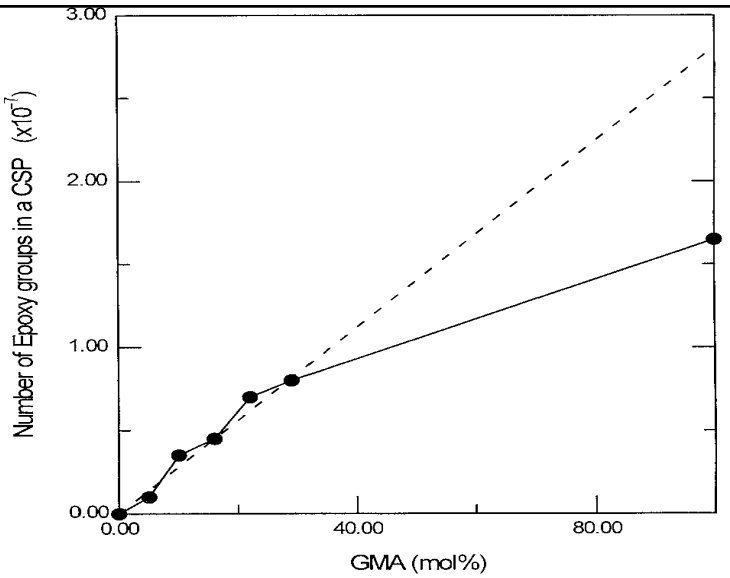

Figure 6 Number of epoxy groups in a particle of the C-series CSP (——) measured by the chemical titration and (---) estimated by eq. (3) as a function of GMA content in the formulations to prepare the shell of the CSP.

Table III Recipes of First-Stage Soapless Emulsion Polymerization for Preparation of Various Sizes of BA Cores for Large CSPs

Component	LBA-1	LBA-2	LBA-3
L-BA (g)	283	—	—
LBA-1 (g)	—	283	—
LBA-2 (g)	—	—	283
BA (g)	20	20	20
Water (g)	547	547	547
KSP (g)	0.2	0.2	0.2

Table IV Recipes of Second-Stage Soapless Emulsion Polymerization for Preparation of Various Sizes of C3-Series CSPs

Component	C3 or C3-0	C3-1	C3-2	C3-3
L-BA (g)	780	—	—	—
LBA-1 (g)	—	780	—	—
LBA-2 (g)	—	—	780	—
LBA-3 (g)	—	—	—	780
MMA (g)	21.5	21.5	21.5	21.5
GMA (g)	6	6	6	6
(mol %)[a]	(16)	(16)	(16)	(16)
EGDMA (g)	0.6	0.6	0.6	0.6
KPS (g)	0.2	0.2	0.2	0.2

[a] Molar percentage of GMA.

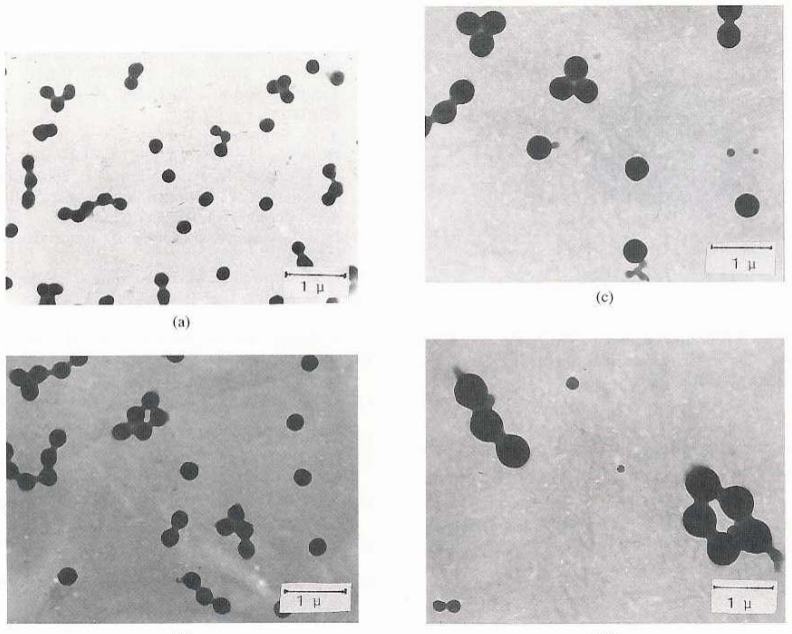

Figure 10 TEM micrographs of vacuum dried (a) C3-0, (b) C3-1, (c) C3-2, and (d) C3-3 CSP.

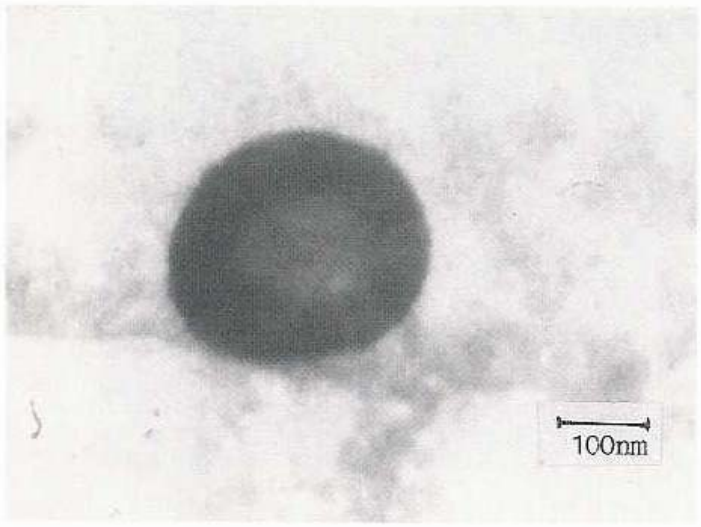

Figure 11 TEM micrograph of RuO_4 stained C3-1 CSP embedded in the epoxy resin, featuring the core–shell structure of the CSP.

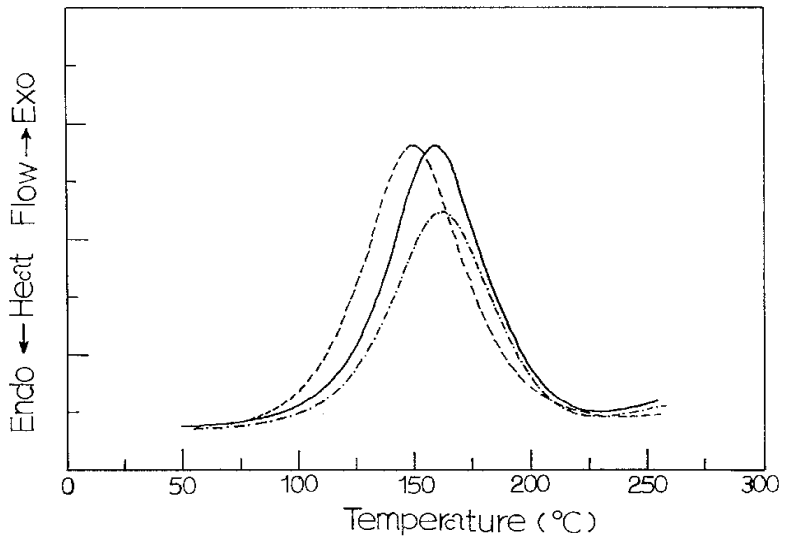

Figure 1 DSC spectra of (——) DGEBA–MPDA, (— · —), DGEBA–MPDA–10 phr C0, and (– – –) DGEBA–MPDA–10 phr C3 epoxy formulations.

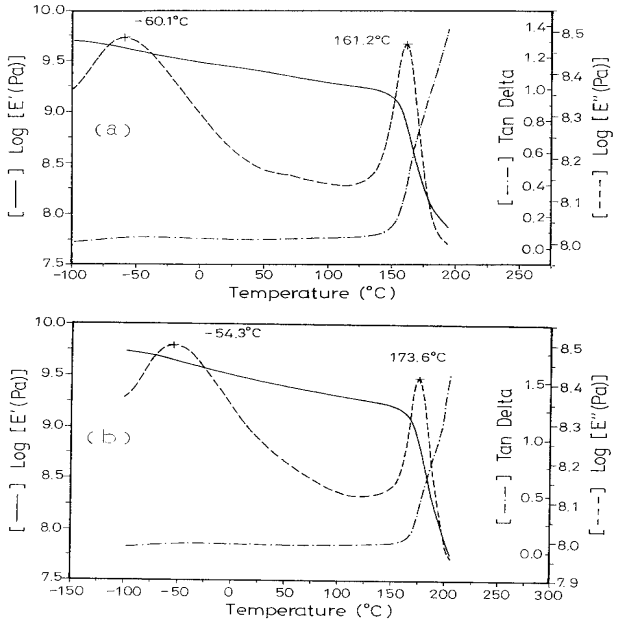

Figure 3 DMA spectra of cured (a) DGEBA–MPDA and (b) DGEBA–MPDA–10 phr C3 epoxy resins.

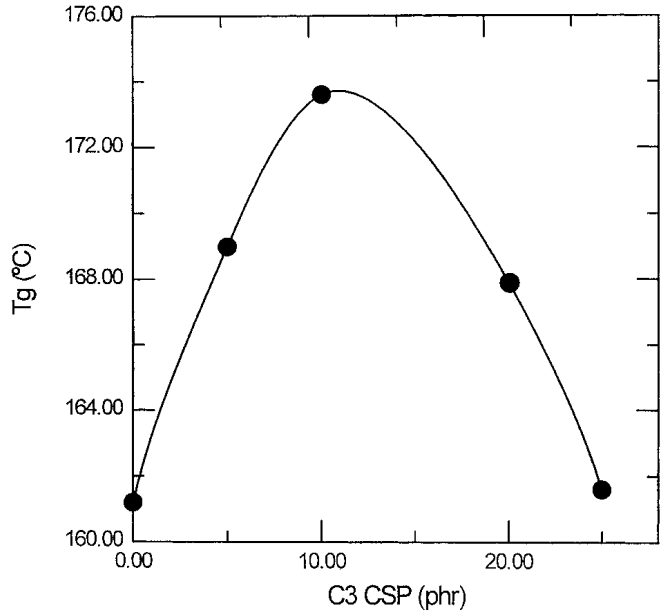

Figure 4 T_g of DGEBA–MPDA–C3 CSP epoxy resins as a function of the C3 CSP content.

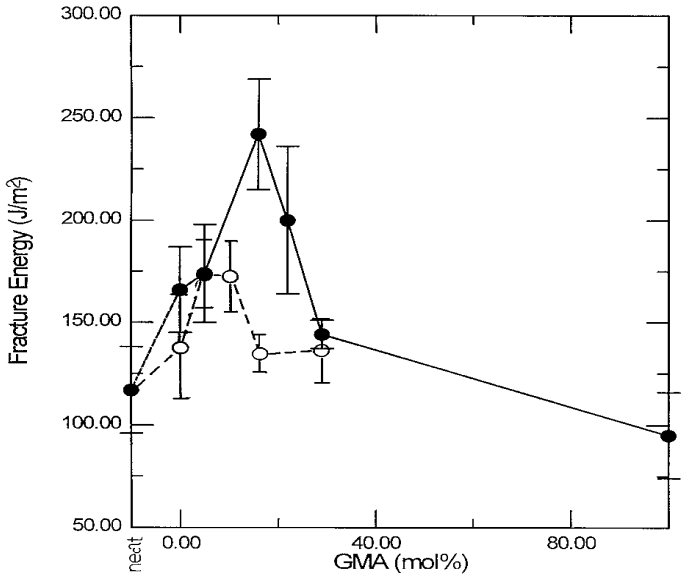

Figure 6 Fracture energy of DGEBA–MPDA epoxy resins incorporating 10 phr (●) C-series and (○) L-series CSP, respectively, as a function of their GMA content in the shell region.

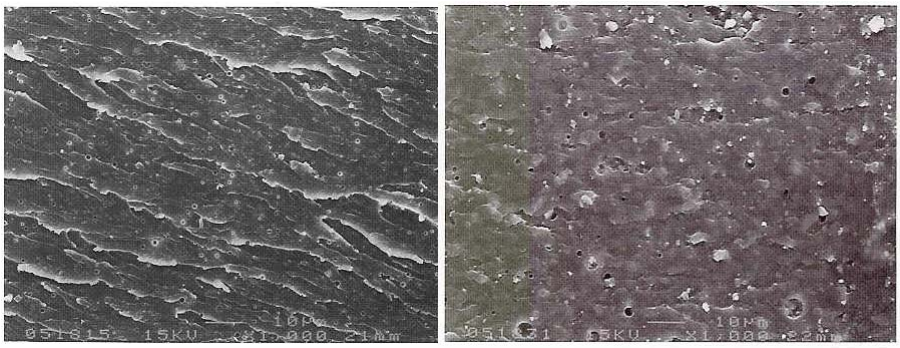

(a) (b)

Figure 7 SEM micrographs of CTS fracture surfaces of (a) DGEBA–MPDA–10 C0 CSP, (b) DGEBA–MPDA–10 C3 CSP, and (c) DGEBA–MPDA–10 C5 CSP epoxy resins.

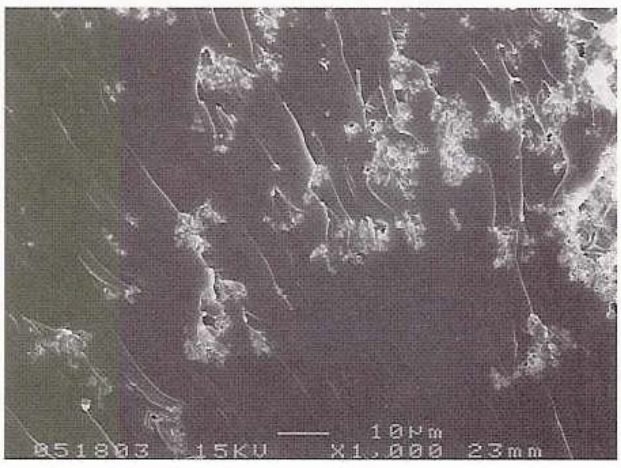

(c)

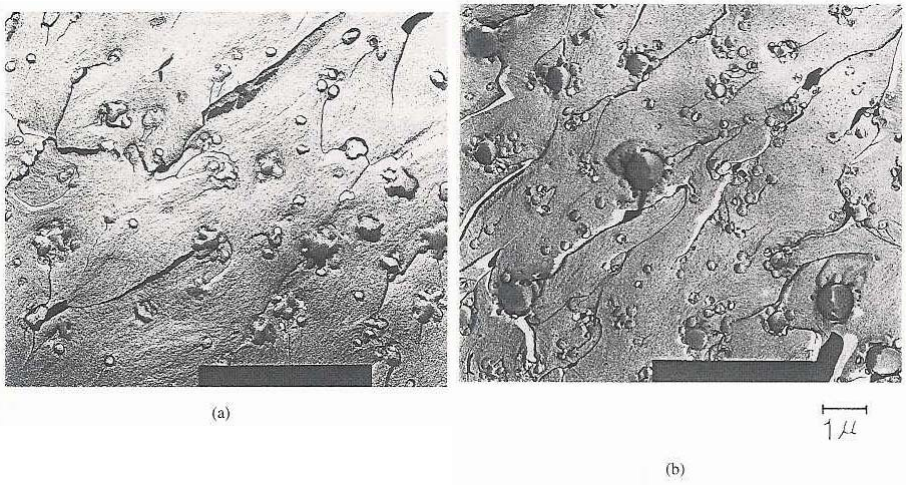

Figure 8 TEM micrographs of one-stage C–Pt replica of CTS fracture surfaces of (a) DGEBA–MPDA–10 C2 CSP and (b) DGEBA–MPDA–10 C3 CSP epoxy resins.

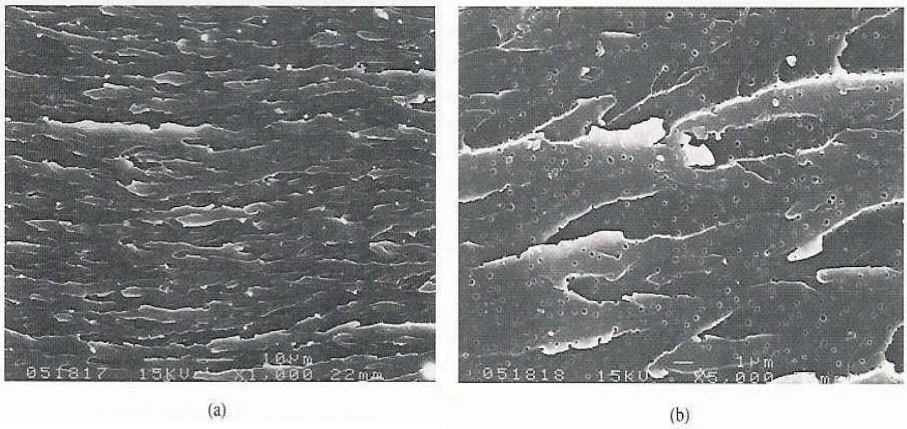

Figure 9 SEM micrographs of CTS fracture surface of DGEBA–MPDA–10 L1 CSP epoxy resin with magnifications of (a) ×1000 and (b) ×5000.

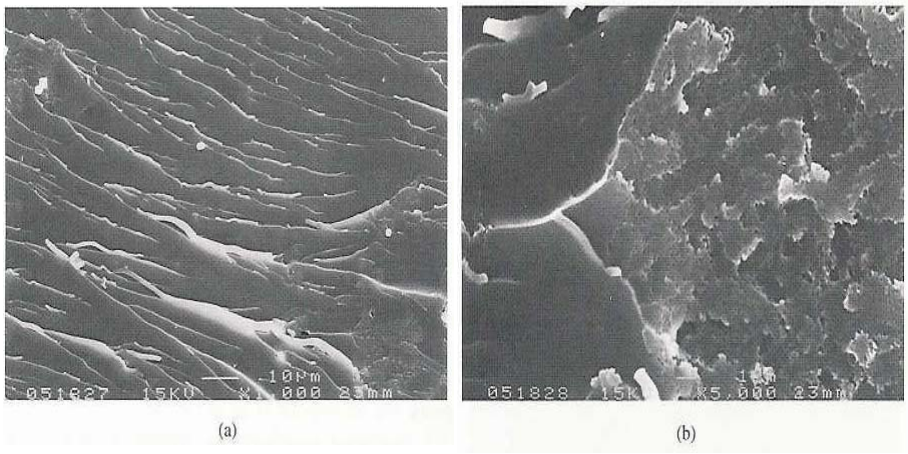

Figure 10 SEM micrographs of CTS fracture surface of DGEBA–MPDA–10 L4 CSP epoxy resin with magnifications of (a) ×1000 and (b) ×5000.

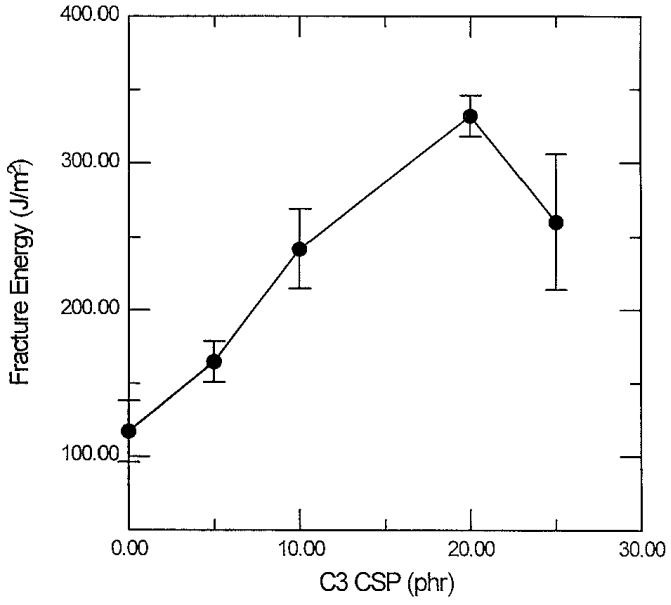

Figure 11 Fracture energy of DGEBA–MPDA–C3 CSP epoxy resins as a function of their CSP content.

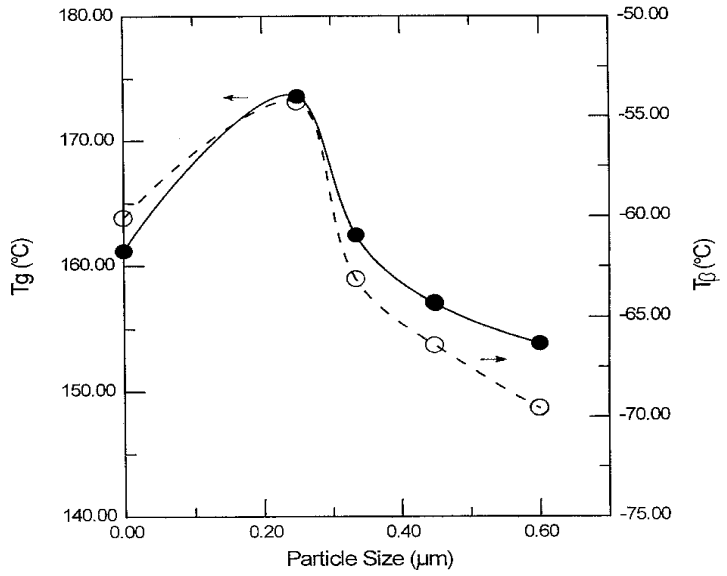

Figure 5 (●) T_g and (○) T_β of DGEBA–MPDA incorporating 10 phr C3-series CSP as a function of their particle size.

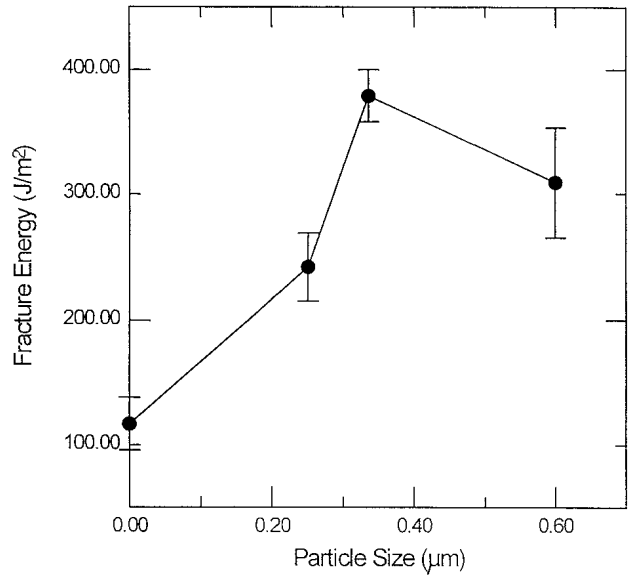

Figure 12 Fracture energy of DGEBA–MPDA incorporating 10 phr C3-series CSP as a function of their particle size.

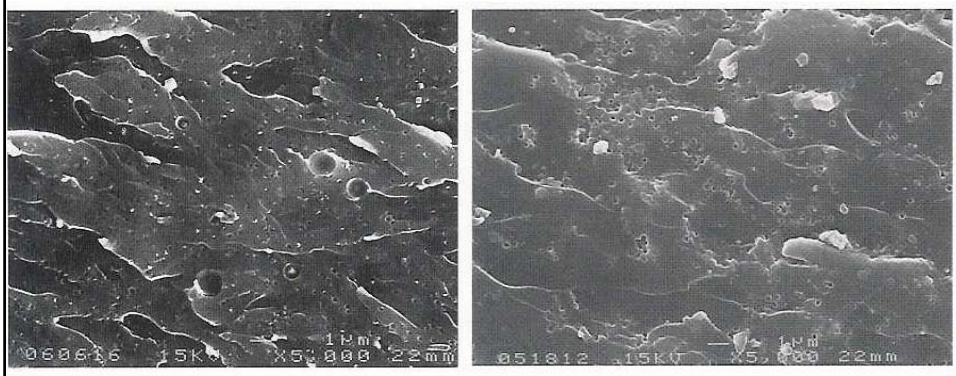

(a) (b)

Figure 13 SEM micrographs of CTS fracture surfaces of (a) DGEBA–MPDA–10 C3-0 CSP, (b) DGEBA–MPDA–10 C3-1 CSP, and (c) DGEBA–MPDA–10 C3-3 CSP epoxy resins.

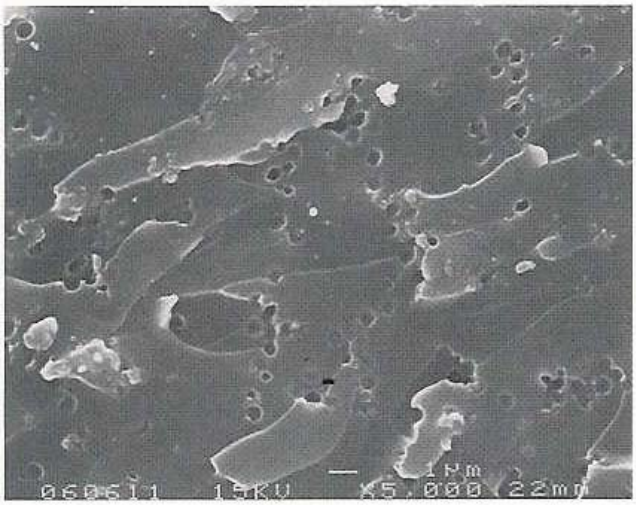

(c)

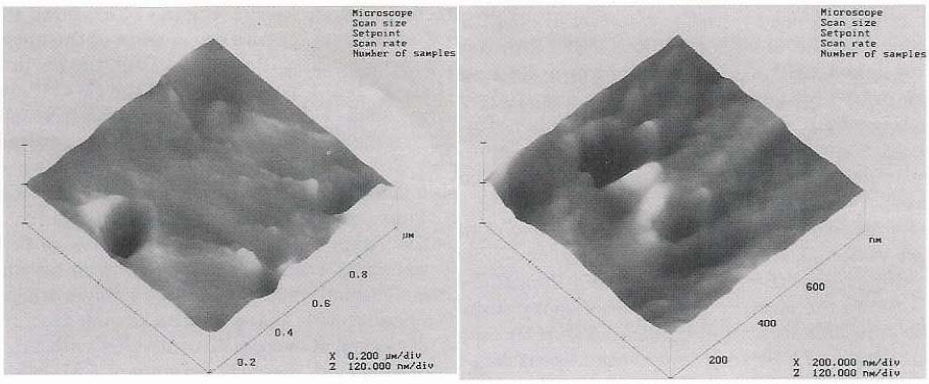

Figure 14 AFM micrographs of CTS fracture surfaces of (a) DGEBA–MPDA–10 C0 CSP, (b) DGEBA–MPDA–10 C3-0 CSP, and (c) DGEBA–MPDA–10 C3-1 CSP epoxy resins.

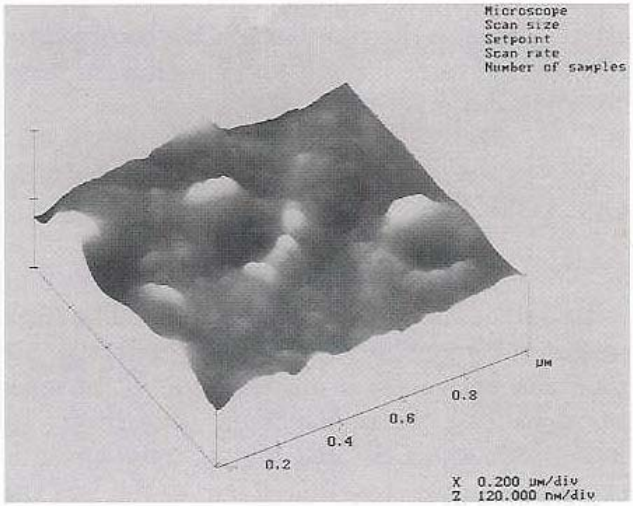

(c)

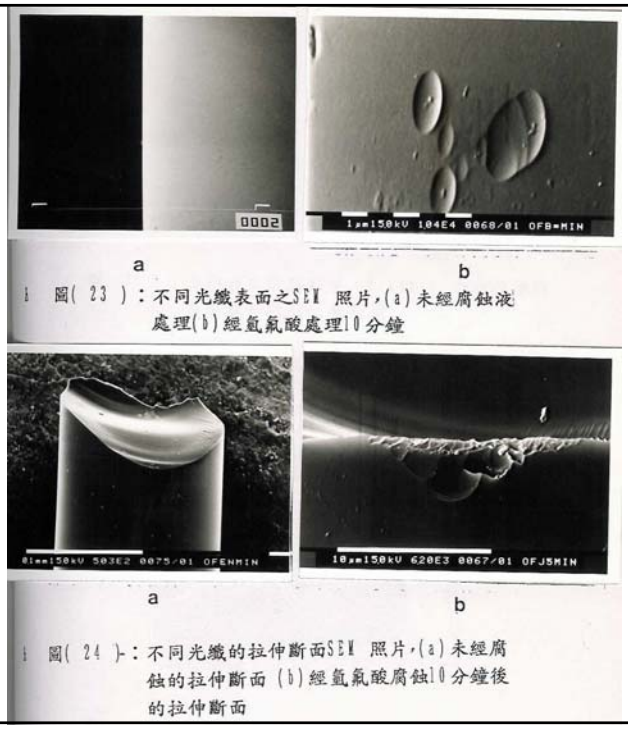

圖(23)：不同光纖表面之SEM 照片，(a)未經腐蝕液處理(b)經氫氟酸處理10分鐘

圖(24)：不同光纖的拉伸斷面SEM 照片，(a)未經腐蝕的拉伸斷面 (b)經氫氟酸腐蝕10分鐘後的拉伸斷面

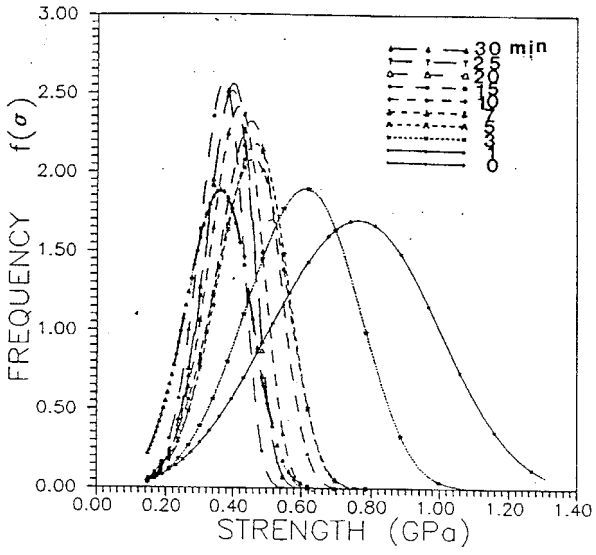

圖(20)：光纖經不同時間氫氟酸腐蝕後，斷裂頻率對拉伸強度之關係圖

1.2.1.1 Weibull 統計法

Weibull 統計法主要以脆性材料弱連結理論(Weak-link theory) 爲基礎，因其可用來分析表面缺陷分佈與拉伸強度的關係，所以經常被用來分析脆性材料的拉伸強度。在Weibull統計模型中，纖維長度L在應力σ以下之累加斷裂機率F，由式(1) 表示：

$$F = 1 - \exp[-L(\sigma / \sigma_0)^m] \quad (1)$$

其中m爲形狀參數（又稱缺陷分佈參數或 Weibull 模數），而 σ_0 爲規格參數（又稱標準化應力）。爲了計算參數 m 及 σ_0 ，將式 (1) 移項重排，取兩次自然對數，得線性函數(2)：

$$\ln[1/L \ln(1/1-F)] = m \ln\sigma - m \ln\sigma_0 \quad (2)$$

以 $\ln[1/L \ln(1/1-F)]$ 對$\ln\sigma$做圖，由直線的斜率及截距可求得m 及σ_0 。若將式 (1) 對拉伸強度σ微分，則可得

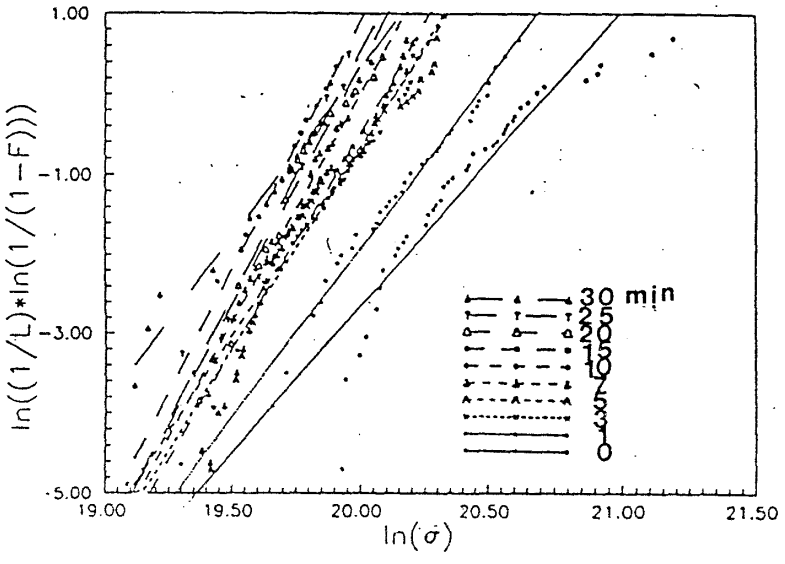

圖(18)：光纖經不同時間氫氟酸腐蝕後，
$\ln(1/L \cdot \ln(1/1-F))$ 對$\ln\sigma$的關係圖

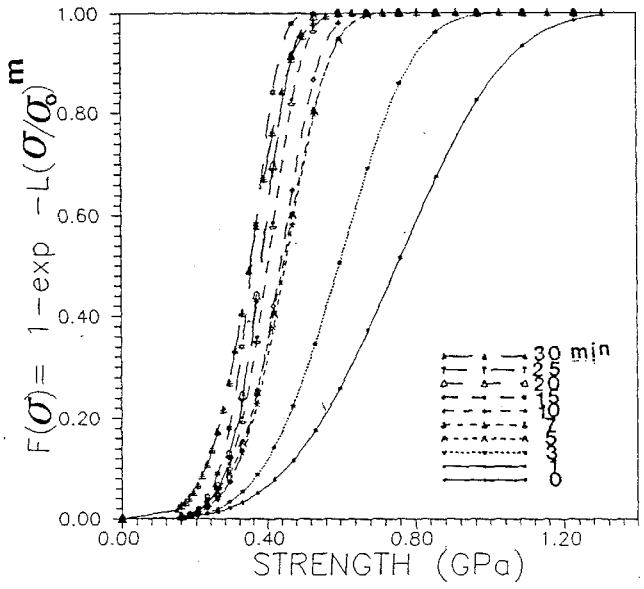

圖(19)：光纖經不同時間氫氟酸腐蝕後，累加斷裂機率對拉伸強度的關係圖

斷裂頻率（又稱機率密度）f(σ) 爲：

$$f(\sigma) = \frac{mL \times \sigma^{m-1}}{\sigma_0^{m}} \exp\left[-L(\sigma/\sigma_0)^{m}\right]$$

平均拉伸強度 $\overline{\sigma}$ 則可由下式計算而得：

$$\overline{\sigma} = \int_0^{\infty} \exp\left[-L(\sigma/\sigma_0)^{m}\right] d\sigma$$

$$= \sigma_0 L^{-1/m} * \Gamma(1+1/m)$$

其中Γ表示Gamma 函數，可由數學手册[17] 中查得。

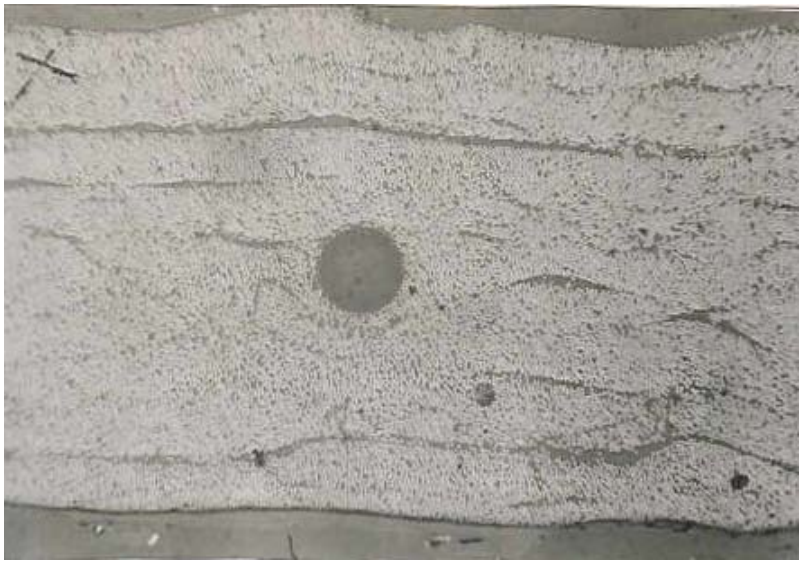

$[\pm 0^o]_4$

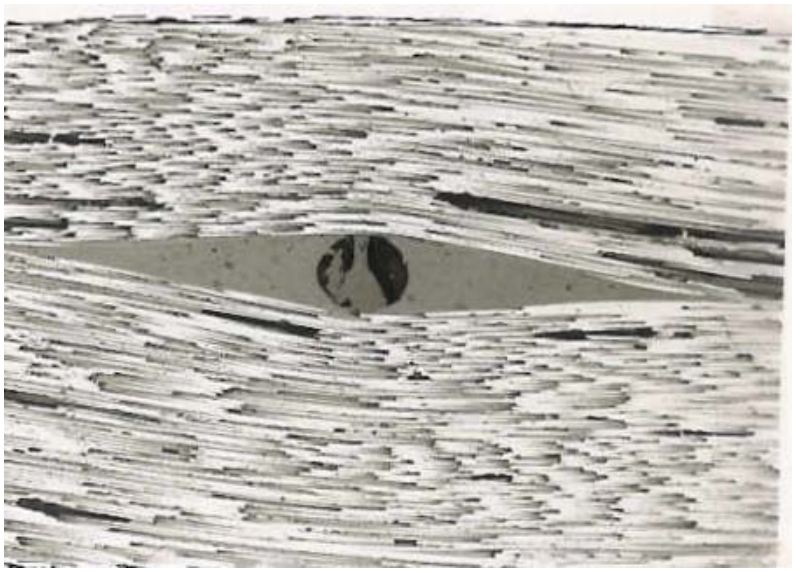

$[\pm 90^o]_4$

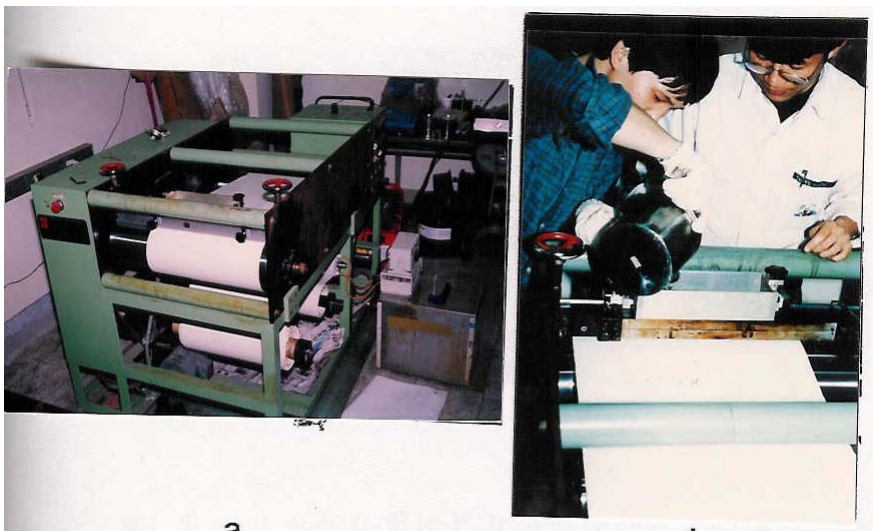

圖(8):(a)塗佈機和(b)將樹脂塗佈於離 型紙的過程

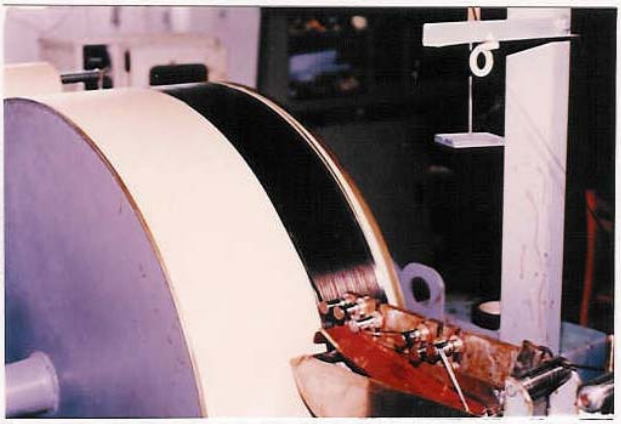

圖(9):熱熔法製造單方向預浸帶時，碳纖維纏繞於鼓輪的作業情形

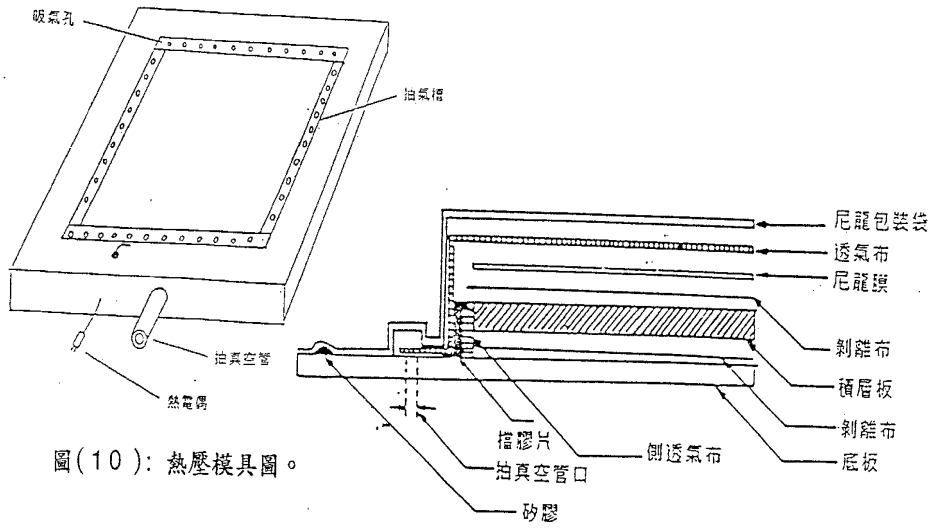

圖(10): 熱壓模具圖。

圖(11): 積層板眞空包裝封袋圖。

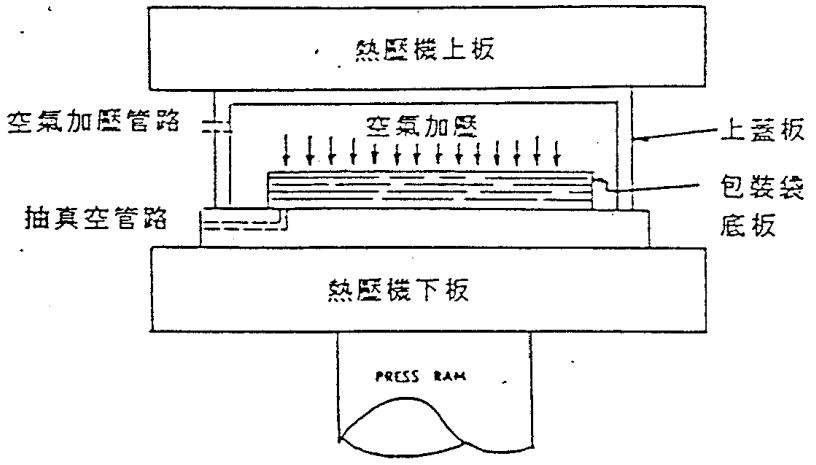

圖(12): 熱壓機改良之熱壓釜。

MTS夾頭部份

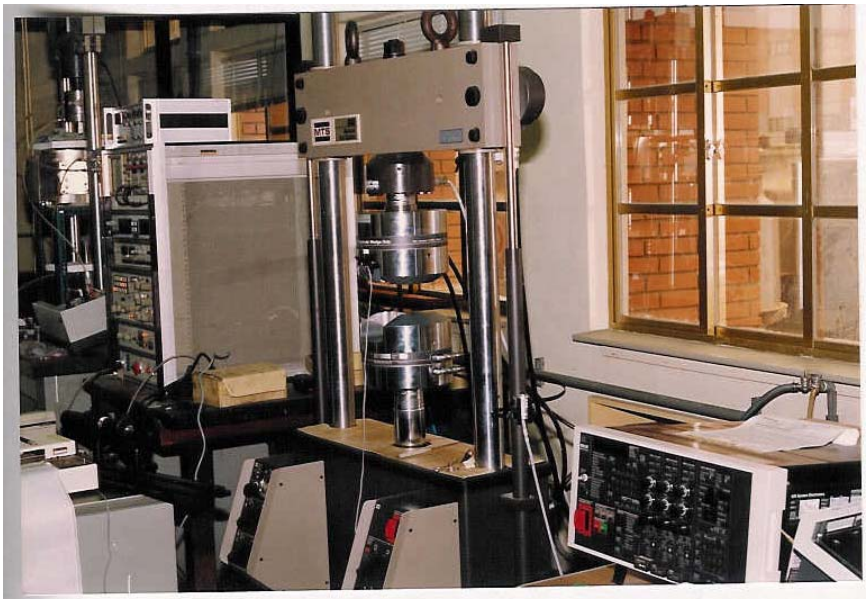

圖(15)：光纖檢驗複合材料結構損傷之裝置圖

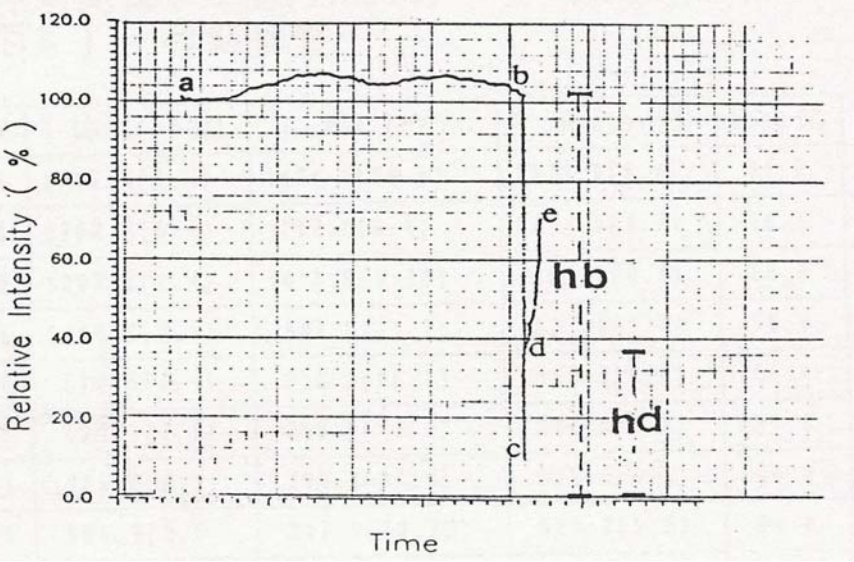

圖(43)：試片在慢速拉伸過程中，光訊的相對強度變化

圖(34)：各種[±θ]$_4$積層板試片，拉伸斷裂後的照片

四、 利用包埋光纖非破壞檢測航空用複合材料結構之損傷

1. 摘 要

將包埋光纖與Gr/Ep積層板一體成形不但對複合材料的機械性質影響不大，而且可偵測到複材受撞擊時結構損傷的情形。本研究利用C-Scan測量複材受撞擊時結構破壞的面積，再與包埋光纖所測量的面積做比較，發現兩者相差不多。利用包埋光纖最大的好處是航空器在使用狀態下仍能偵測到結構損傷的情形。

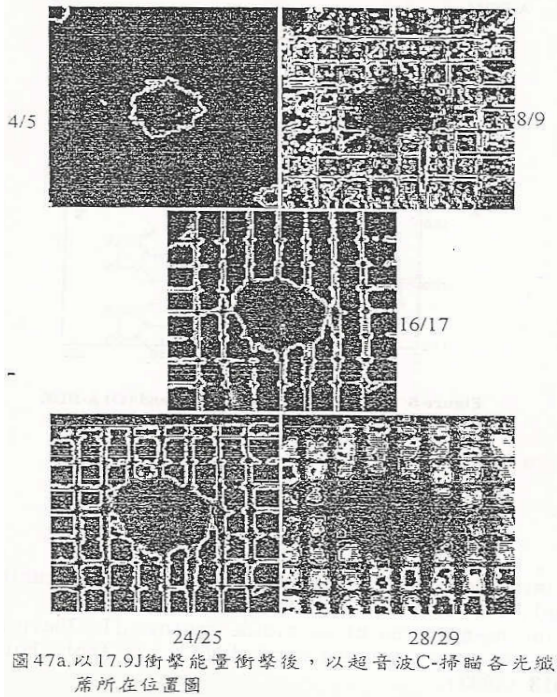

圖47a.以17.9J衝擊能量衝擊後，以超音波C-掃瞄各光纖所在位置圖

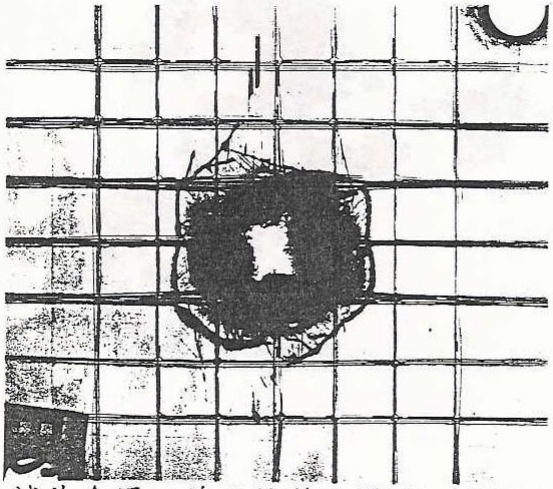

同一試片含浸四溴乙烷後，X-光　所顯示的破壞面積

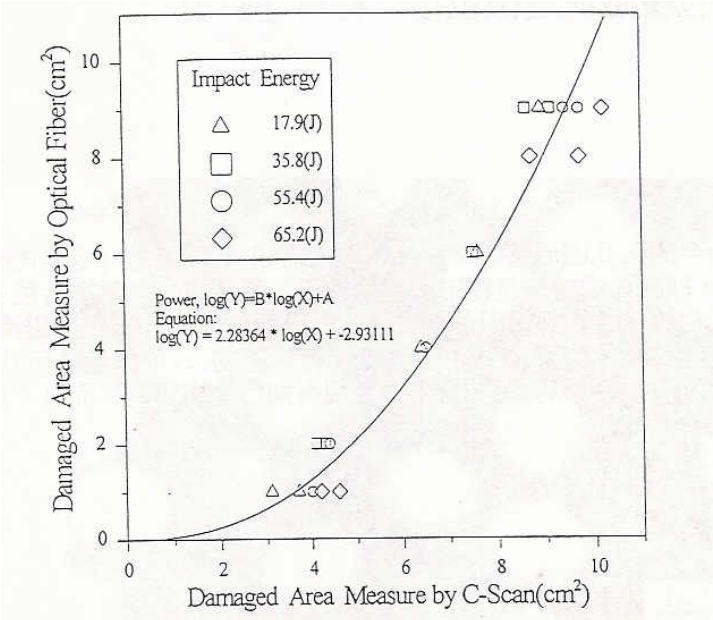

圖48.以光纖所估計和C-掃瞄所估計各層破壞的面積對應圖(圖中符號表示測試所使用能量)